Glacial cycle ice-sheet evolution controlled by oceanbed properties

Clemens Schannwell[1], Reinhard Drews[2], Todd Ehlers[3], Olaf Eisen[4], Christoph Mayer[5], Mika Malinen[6], Emma Clare Smith[7], and Hannes Eisermann[8]

[1]Max Planck Institute for Meteorology
[2]Department of Geosciences, University of Tübingen
[3]University of Tubingen
[4]Alfred Wegener Institute Helmholtz Center for Polar and Marine Research
[5]Bavarian Academy of Sciences and Humanity
[6]CSC-IT Center for Science Ltd.
[7]Alfred-Wegener-Institut Helmholtz-Zentrum für Polar- und Meeresforschung
[8]Alfred Wegener Institute for Polar and Marine Research

November 21, 2022

Abstract

Improving constraints on the basal ice/bed properties is essential for accurate prediction of ice-sheet grounding-line positions and stability. Furthermore, the history of grounding-line positions since the Last Glacial Maximum has proven challenging to understand due to uncertainties in bed conditions. Here we use a 3D full-Stokes ice-sheet model to investigate the effect of differing ocean bed properties on ice-sheet advance and retreat over a glacial cycle. We do this for the Ekström Ice Shelf catchment, East Antarctica. We find that predicted ice volumes differ by >50%, resulting in two entirely different catchment geometries triggered exclusively by variable ocean bed properties. Grounding-line positions between simulations differ by >100% (49 km), show significant hysteresis, and migrate non-steadily with long quiescent phases disrupted by leaps of rapid migration. These results highlight that constraints for both bathymetry and substrate geologic properties are urgently needed for predicting ice-sheet evolution and sea-level change.

Glacial cycle ice-sheet evolution controlled by ocean bed properties

C. Schannwell[1*], R. Drews[1], T.A. Ehlers[1], O. Eisen[2,3], C. Mayer[4], M.Malinen[5], E.C. Smith[2], and H. Eisermann[2]

[1]Department of Geosciences, University of Tübingen, Tübingen, Germany
[2]Glaciology, Alfred Wegener Institute, Helmholtz Centre for Polar and Marine Research, Bremerhaven, Germany
[3]Department of Geosciences, University of Bremen, Bremen, Germany
[4]Bavarian Academy for Sciences and Humanities, Munich, Germany
[5]CSC-IT Center for Science Ltd., Espoo, Finland

Key Points:

- Ocean bed properties exert a critical control on ice-sheet geometry over full glacial cycle
- Ice thickness and grounding-line position differ by up to 1000 m and 50 km between hard-bed and soft-bed simulations
- Ice-sheet change is characterized by short periods of advance or retreat followed by long periods of ice-sheet stability

*Now at: Max Planck Institute for Meteorology, Bundesstraße 53, 20146 Hamburg, Germany

Corresponding author: Clemens Schannwell, `Clemens.Schannwell@mpimet.mpg.de`

Abstract

Improving constraints on the basal ice/bed properties is essential for accurate prediction of ice-sheet grounding-line positions and stability. Furthermore, the history of grounding-line positions since the Last Glacial Maximum has proven challenging to understand due to uncertainties in bed conditions. Here we use a 3D full-Stokes ice-sheet model to investigate the effect of differing ocean bed properties on ice-sheet advance and retreat over a glacial cycle. We do this for the Ekström Ice Shelf catchment, East Antarctica. We find that predicted ice volumes differ by >50%, resulting in two entirely different catchment geometries triggered exclusively by variable ocean bed properties. Grounding-line positions between simulations differ by >100% (49 km), show significant hysteresis, and migrate non-steadily with long quiescent phases disrupted by leaps of rapid migration. These results highlight that constraints for both bathymetry and substrate geologic properties are urgently needed for predicting ice-sheet evolution and sea-level change.

Plain Language Summary

The Antarctic ice sheet is completely surrounded by oceans. However, what type of rock is at the bottom of these oceans is poorly known. During previous glaciations the ice sheet has advanced and retreated multiple times over areas of contemporary oceans. As the ice comes into contact with the ocean floor, friction between ice and ocean floor determines how fast the ice flows and influences the ice-sheet size and shape. Here we present computer simulations of the Ekström Ice Shelf, East Antarctica, that show the importance of the type of rock at the bottom of contemporary oceans for ice sheet advance and retreat. Our simulations reveal that different materials could result in a 50% volume difference. Even though Ekström Ice Shelf is relatively small, there is evidence that similar conditions are present over large areas surrounding the Antarctic ice sheet. This means that the Antarctic ice sheet might have looked very different during past glaciations than previously thought.

1 Introduction

Shortcomings in the description of ice dynamics have been recognized as a major limitation for projecting the evolution of the Greenland and Antarctic ice sheets (IPCC AR5, Pachauri et al., 2014). If present sea-level rise rates continue unabated, up to 630 million people will be at annual flood risk by 2100 (Kulp & Strauss, 2019), making improved ice-sheet model projections a priority of high socioeconomic impact. The current state-of-the art for long-term (>1,000 year) ice-sheet simulations requires simplifications in the ice-dynamical equations that result in two limitations. First, it is questionable whether the transition zone between grounded and floating ice (e.g. the grounding zone) is adequately represented in existing long-term simulations (Schoof, 2007). Second, the omission of membrane and bridging stress gradients hamper disentangling the relative contributions of basal sliding and ice deformation to the column averaged ice discharge (MacGregor et al., 2016; Bons et al., 2018). The former is one of the main uncertainties for projecting the sea-level contribution of contemporary ice sheets (Durand et al., 2009; Pattyn & Durand, 2013). The latter is a bottleneck for the inclusion of basal processes such as erosion and deposition of sediments which critically depend on the magnitude of basal sliding (e.g., Humphrey & Raymond, 1994; Egholm et al., 2011; Herman et al., 2011; Yanites & Ehlers, 2016; Alley et al., 2019) and may govern the formation and decay of ice streams (Spagnolo et al., 2016).

Recently, a number of simplified model variants of the full ice-flow equations have been successfully applied to sea-level rise projections using ensemble simulations that account for uncertainties in atmospheric and oceanic boundary conditions over timescales of >1,000 years (e.g., Golledge et al., 2012; Briggs et al., 2014; Pollard et al., 2016). More realistic full-Stokes simulations, on the other hand, have thus far only been applied to a maximum of 1,000 years for real-world geometries due to the high computational demands, both, in terms of mesh resolution and the physics required to solve for a freely evolving grounding line (Gillet-Chaulet et al., 2012; Seddik et al., 2012; Favier et al., 2014; Schannwell et al., 2019).

A particular challenge that arises in model simulations over long time scales (≥40,000 years) is that the ice sheet advances and retreats over ocean beds where bathymetry and its geological properties are often poorly known. While the slopes of the ice-shelf cavity and the bed topography farther upstream have received much attention because of their control on ice-sheet stability (e.g., Schoof, 2007; Tsai et al., 2015), comparatively little research has focused on the corresponding geological properties controlling basal sliding or the lack thereof. Estimating basal friction parameters under contemporary ice sheets (e.g. basal friction between the ice sheet and the underlying substrate) is virtually impossible by direct measurements and can only be inferred indirectly on a continental scale by solving an optimization problem matching todays surface velocities and/or ice thickness (e.g., MacAyeal, 1993; Gillet-Chaulet et al., 2012; Cornford et al., 2015). Furthermore, the inferred basal friction coefficient is often spatially heterogeneous and can vary by up to five orders of magnitude under the present-day Antarctic ice sheet (Cornford et al., 2015). To what extent this variability truly reflects variability in geology, or is falsely introduced by the approximations in the ice-dynamical equations or omission of ice anisotropy is unknown. Even less is known about the properties of ocean beds under contemporary ice shelves. In previous sensitivity studies, basal properties of ocean beds have been identified as a major source of uncertainty in ice-dynamic models (e.g., Pollard & DeConto, 2009; Pollard et al., 2016; Albrecht et al., 2019). However, the lack of a comprehensive Antarctic-wide distribution map of sedimentary deposits and crystalline rock, together with the absence of a full-Stokes model over the time scales required, leaves characterization of basal friction parameters and their consequences for ice-sheet growth and decay poorly constrained.

Here we employ a three-dimensional (3D), isotropic, thermomechanically-coupled full-Stokes model (Elmer/Ice, Gagliardini et al. (2013)) to narrow the time gap between projections from simplified model simulations over long timescales, and ice-dynamically more complete simulations over shorter time scales. We do this with a highly parallelized numerical scheme allowing to maintain a high mesh resolution (∼1 km) and a freely evolving grounding line over glacial/interglacial timescales. Our simulations focus on the effect of ocean bed properties seawards of today's grounding line and to quantify their impact on the evolution of the entire catchment. This is done for the Ekström Ice Shelf catchment, Dronning Maud Land, East Antarctica (Fig. 1), containing multiple ice rises and pinning points (Schannwell et al., 2019; Drews et al., 2013), and hosting Neumayer Station III. Uncertainties in the contemporary ice-sheet geometry are minimal because of previous dense airborne radar surveys in the vicinity of Neumayer Station III (Fretwell et al., 2013). Unlike many other ice shelves, the bathymetry in this area is known to a high accuracy, across much of the sub-ice-shelf, from extensive seismic reflection surveying (Smith et al., 2019). This has been extended to cover the whole cavity by aero-gravimetry measurements (H. Eisermann 2019, personal communication). Furthermore, there is evidence in this area from multiple geophysical observations about contrasting ocean bed properties (Kristoffersen et al., 2014). While much recent research has focused on the fast flowing outlet glaciers of Antarctica, we stress the importance of also studying catchments characterised by slower moving ice (<300 m/yr), as they occupy ∼90% of the contemporary Antarctic grounding line and account for 30% of the total ice discharge (see SI, sec. 5; Bindschadler et al., 2011; Rignot et al., 2011).

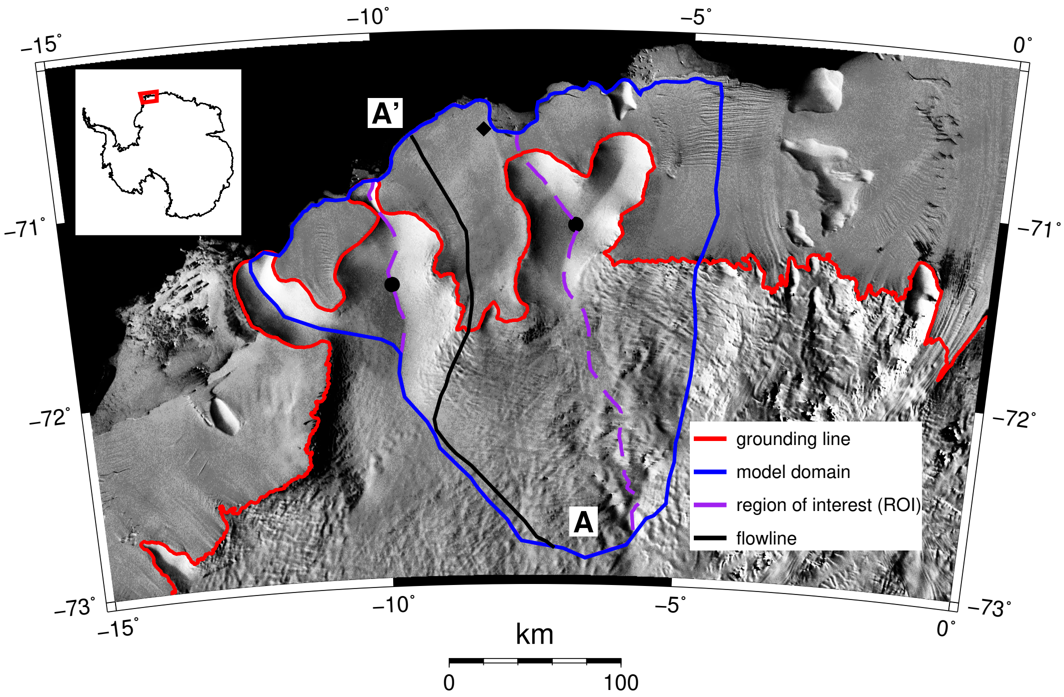

Figure 1. Overview of the Ekström Ice Shelf catchment with present-day grounding line and model domain. Black square shows location of Neumayer Station III. Filled black circles indicate location of ice rises. Flowline (A-A') is shown in Fig. 4.

The results we obtain for the Ekström Ice Shelf catchment are therefore relevant for many other catchments around Antarctica and hence the total budget.

2 Materials and Methods

2.1 Ice sheet model and external forcing

We use the transient, thermomechanically-coupled full-Stokes model Elmer/Ice (Gagliardini et al., 2013). The finite element model solves the full ice-flow equations in 3D for ice deformation and incorporates a freely evolving grounding line without parameterizations. The equations are solved on a model grid that has a background resolution of 6 km, and is locally refined down to 1 km at today's grounding line and seaward of today's grounding line at the Ekström Ice Shelf. Subglacial topography is taken from Bedmap2 (Fretwell et al., 2013) for the grounded ice sheet, but updated for the bathymetry underneath Ekström Ice Shelf based on recent seismic surveys and aero-gravimetry (H. Eisermann 2019, personal communication). Underneath ice shelves outside the area of interest, the Bedmap2 bathymetry is lowered by ∼300 m to ensure that the ice shelf is floating, as Bedmap2 is unrealistically shallow. Our present day surface elevation is a merged product of CryoSat-2 and, where available, higher-resolution TanDEM-X digital elevation models (Schannwell et al., 2019). Ice temperature is initialized to a steady state for present-day conditions (see SI, sec. 2.4; Zhao et al., 2018; Rückamp et al., 2018). The temperature model is forced at the ice surface by a present-day temperature distribution (Comiso, 2000) plus a temporal surface temperature change that is derived from the nearby EDML ice core (Graf et al., 2002), located some 700 km to the south-east of the region of interest (ROI; Fig. 1) on the Antarctic plateau. At the grounded basal boundary, a spatially variable but time-invariant heat flux is prescribed (Martos et al., 2017), while ice temperature is set to the pressure-melting-point at the bottom of floating ice. The surface mass balance (SMB) parameterization follows Ritz et al. (2001). We apply a present-day SMB field (Lenaerts et al., 2014). Temporal change in the SMB is proportional to the exponential of surface temperature change (see SI, sec. 2.3.2). The basal mass balance (BMB) applied at the ice-shelf underside is proportional to the square of the temperature difference between the ice-shelf underside and the ocean temperature at the continental shelf edge (Beckmann & Goosse, 2003). Ocean temperature variations are a damped (∼40%) and delayed (∼3,000 years) version of the surface temperature variation (Bintanja et al., 2005). Sea level is varied according to Lambeck et al. (2014) which includes isostatic and tectonic contributions. Underneath the grounded ice sheet, we apply a linear Weertman-type sliding law.

2.2 Experimental design

We investigate ice-sheet growth and decay over 40,000 years. During the first 20,000 years the atmospheric and oceanic forcing simulates the transition from an interglacial to a glacial (henceforth called the advance phase). We then symmetrically reverse the climate forcing to simulate deglaciation (henceforth called the retreat phase). The symmetrical reversal of the model forcing enables investigation of hysteresis effects. The interglacial starting conditions are chosen with present day properties and characteristics, so that the best possible basal friction coefficient beneath the grounded ice sheet can be found using today's ice-sheet geometry and surface velocities (Schannwell et al., 2019). The glacial conditions are chosen to resemble the Last Glacial Maximum for which we have good constraints for atmospheric forcing from the nearby EDML ice core. We consider two end-member basal-property scenarios by prescribing either soft ocean bed conditions (mimicking sediment deposits) or hard ocean bed conditions (mimicking crystalline rock) for all present-day ocean cavities in the modelling domain. The tested end-member scenarios of basal traction coefficients encompasses what other ice-sheet models have inferred (e.g., Cornford et al., 2015) for the grounded portion underneath the present-day Antarctic ice sheet (basal traction coefficient ranging from 10^{-1} MPa m^{-1} yr for sediments to 10^{-5} MPa m^{-1} yr for crystalline bedrock). This means that simulated differences in ice volume and grounding-line position should be interpreted as the maximum envelope of uncertainties resulting from different ocean bed properties. We perform the simulations with a) the standard Elmer/Ice setup using the Multifrontal Massively Parallel Sparse (MUMPS) direct solver for ice velocities; and b) using a stable iterative solver for ice velocities (see SI, sec. 2.6; Malinen et al., 2013), resulting in a total of four simulations.

3 Results and Discussion

3.1 Influence of bed hardness on ice-sheet growth and decay

The two scenarios of hard vs. soft bed result in two fully different ice sheet geometries at the glacial maximum with different volumes (Fig. 2), fluxes, and grounding line positions through time (Figs. 3 and 4). For example, the simulated hard bed ice sheet is in many areas more than twice as thick as the soft bed ice sheet, with maximum ice thickness differences between hard and soft bed reaching 1,036 m or 120% (Fig. 3). In more detail, the differences between these simulations are as follows:

First, the hard bed ice sheet results in a thick, slow, and large volume ice sheet after 20,000 years at glacial conditions. During the advance phase, volume increases occur step-wise with three distinct periods of volume increases (Fig. 2). These periods of volume increase in the ROI are short (<2000 years) and are interrupted

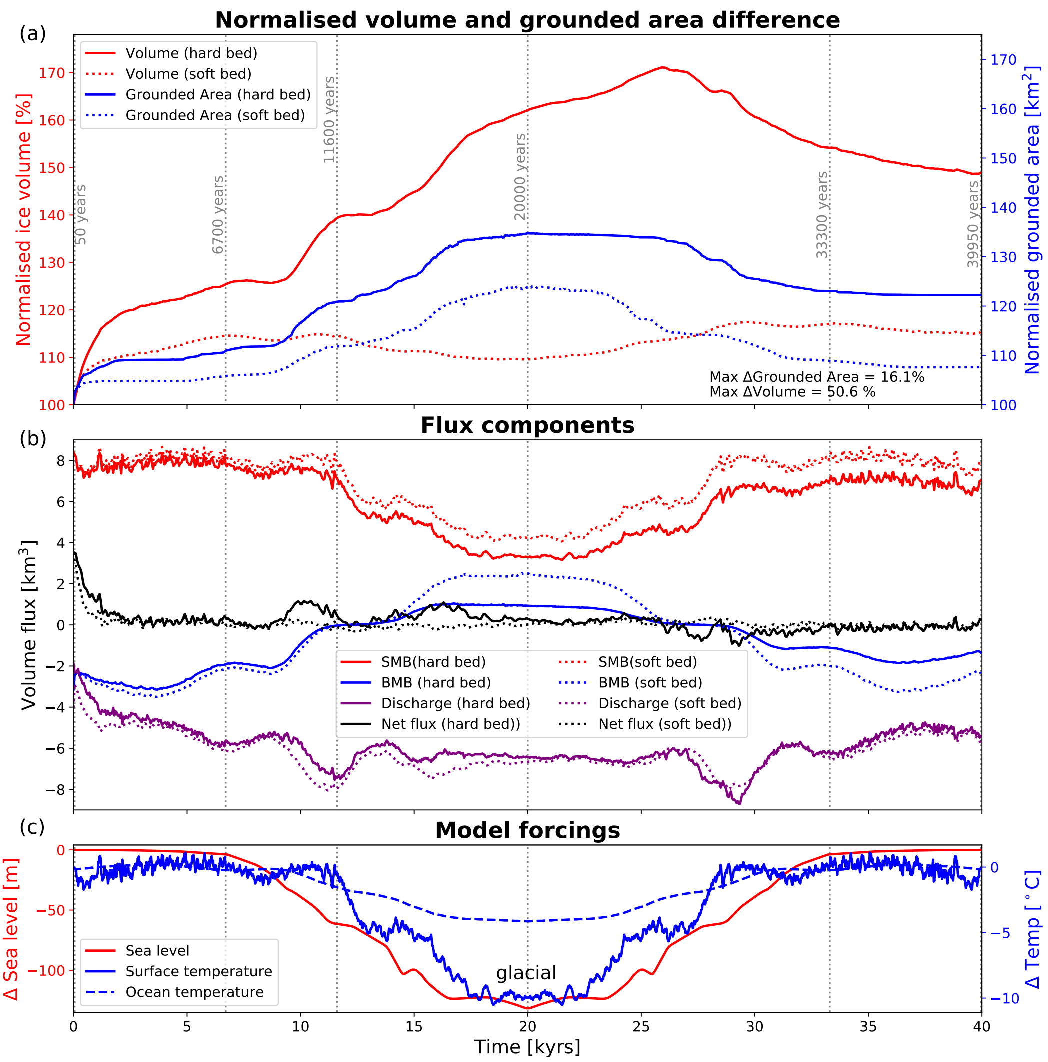

Figure 2. Ice-sheet evolution and model forcing for soft and hard-bed simulations. (a) shows volume and grounded area evolution normalsied to present-day. (b) shows corresponding mass balance fluxes, and (c) shows most important model forcings. Vertical grey stippled lines show time slices shown in Figs. 3 and 4.

by longer periods of little ice volume change. At the glacial maximum, the volume increase in comparison to the interglacial is ∼60%. During the first ∼8,000 years in the retreat phase, the hard bed simulation continues to gain volume albeit at a slow rate. The continued raising of the sea level finally forces the hard bed ice sheet to start losing volume. However, the rate of volume loss is small, such that after a full glacial cycle, the total ice volume is still ∼47% more of what is was at the beginning of the simulation. This relative stability of the hard-bed ice sheet during the retreat phase is a consequence of the higher levels of basal friction provided by the hard bed.

Second, unlike the hard-bed simulations, the soft-bed simulation leads to a thin, fast, and small volume ice sheet at glacial conditions. During the advance phase, this simulation does not show a step-wise volume gain pattern. In fact, apart from an initial volume gain in the first 1,000 years of the advance phase (∼10%), there is very little volume change. This leads to a volume increase of merely ∼8% at the glacial maximum. The trend of little volume variations continues during the retreat phase, where in the first 10,000 years a volume increase of ∼8% occurs, before the volume remains approximately constant for the remainder of the retreat phase.

The entirely different ice-sheet geometries for soft and hard-bed simulations have consequences for the two ice rises present in the catchment (Fig.1). While both ice rises and their divide positions are very little affected by the soft bed simulations, they are partly overrun in the hard bed simulation such that their local ice flow centre vanishes (SI video 1).

The predicted differences between the hard-bed and soft-bed simulations underline the high significance of a proper choice of basal properties used for ocean beds. The higher basal friction in the hard-bed case leads to elevated back stress and corresponding dynamical thickening of the inland ice sheet far upstream of the grounding line. Although the SMB and BMB forcings equally depend on the ice-sheet geometry through the applied parameterizations, these effects are small compared to the ice-dynamically induced thickening (Fig. 3). This clearly shows that in the absence of other forcing mechanisms, ocean bed properties exert a first-order control on ice-sheet growth and decay. Geomorphological evidence from underneath Ekström Ice Shelf indicates that the grounding line was likely near the shelf front at the LGM (Smith et al., 2019). This observation matches well with our hard-bed simulations.

Owing to the paucity of observational constraints, numerical modelling studies have often applied a binary distribution of sediment-based ocean beds and crystalline-based ocean beds (e.g., Pollard & DeConto, 2009; Whitehouse et al., 2012). Hereby, most of the ocean bed areas surrounding Antarctica are assumed to be sediment-based. However, geophysical observations in our study area and elsewhere in Antarctica (e.g., Gohl et al., 2013; Kristoffersen et al., 2014) indicate a much more heterogeneous substrate distribution of sediment deposits and crystalline bedrock on the continental shelf. Some of these crystalline bedrock features like the Explora Wedge in Dronning Maud Land are more than 1000 km long (Gohl et al., 2013; Kristoffersen et al., 2014). Based on our simulations, such crystalline outcrops under ice shelves will have large impacts on ice thickness and ice volume of the Antarctic ice sheet over the last glacial cycle. The differences in ice volume and ice thickness between hard and soft bed are such that they may help to explain the "missing ice" (Clark & Tarasov, 2014) problem at the LGM, if extrapolated to the Antarctic ice sheet. This problem relates to the fact that current sea-level reconstructions suggest a sea-level drop of ∼130 m at the LGM compared to present-day conditions (Simms et al., 2019). However, reconstructions of all major ice sheets at the LGM only account for ∼114 m of sea-level drop, so that ∼16 m of sea-level equivalent is unaccounted for.

Finally (third), the ramifications of heterogeneous ocean bed properties go beyond ice volume considerations. Different levels of basal traction strongly affect the magnitude of basal sliding. This in turn determines how much material is eroded underneath the ice sheet and transported across the grounding line. As erosion rates are commonly approximated as basal sliding to some power (e.g., Herman et al., 2015; Koppes et al., 2015), any differences in basal sliding velocities are exacerbated when erosion volumes are computed (see SI, sec. 6). This uncertainty in eroded material produced has implications for how much sediment is available at the ice-bedrock interface and therefore if it is a hard- vs. soft-bed interface and its temporal variablity.

3.2 Grounding-line and ice-sheet stability

Stable grounding-line positions for both simulations are associated with periods of ice-sheet stability (Fig. 2). In our simulations, there are three distinct periods of grounding-line stability in the advance phase and one period of grounding-line stability in the retreat phase. All of these four periods are longer than 3,000 years. Periods of grounding-line advance in comparison are characterized by short leaps taking no longer than 1,000-2,000 years (Fig. 2). These stable ice-sheet configurations are not controlled by a single specific forcing alone, but are due to a combination of sea-level forcing, basal traction of the ocean bed, and ocean bathymetry. Other forcing mechanisms such as the SMB and BMB are of secondary importance.

During the advance phase, differences in grounding-line positions between the hard-bed and soft-bed simulations gradually increase from 7 km after ∼1,500 years to over 37 km after 11,600 years, and finally to its maximum difference of 49 km at the glacial maximum (Fig. 4). This means that grounding-line advance for the hard bed is more than twice as far (∼110% larger) than its soft bed counterpart in the advance phase.

In the retreat phase, the soft-bed simulation shows higher grounding-line fidelity compared to the hard-bed simulation. The soft bed starts to exhibit grounding-line retreat after ∼4,000 years into the retreat phase, whereas the hard bed does not show grounding-line retreat for ∼8,000 years into the retreat phase. This can be attributed to the fact that ice discharge for the soft-bed simulation is dominated by basal sliding and higher ice velocities. In comparison, in the hard bed simulation ice discharge is dominated by internal deformation and almost no basal sliding, resulting in a mucher thicker ice sheet. This means that more ice needs to be removed before the grounded ice can detach from its subglacial material and initiate grounding-line motion, thereby resulting in a much slower response time to changes in the model forcing.

While our employed modelling approach make it unlikely that the timing of our modelled stable grounding-line positions are correct, they can still serve as spatial markers of areas where depositional landforms such as Grounding-Zone Wedges (GZWs) may be found. Their height and width can be exploited to estimate the erosive power of the upstream catchment at the time of deposition (Batchelor & Dowdeswell, 2015). Assuming similar supply of subglacial material to the grounding line, the hard-bed case should result in thicker grounding zone wedges, because it exhibits longer periods of grounding-line stability. However, if erosion is approximated by basal sliding to some power, sediment supply should be much higher for the soft-bed simulation (SI Fig. 8), potentially offsetting the effect of higher temporal grounding-line fluctuation. Our calculations indicate that for current erosion laws, this effect could outweigh greater grounding-line stability, but other processes such as sediment transport ought to be considered before a definitive assessment can be made.

3.3 Hysteresis of ice-sheet simulations

Next we compare the ice-sheet history and results from the advance phase and the retreat phase simulations. We focus on the effect of basal properties and their impact on ice-sheet hysteresis. After a full glacial cycle in which atmospheric and oceanic forcing are essentially symmetrically reversed for the advance and retreat phase, both of our simulations show hysteresis because the ice sheet does not return to its initial geometry. However, the hysteresis effect is smaller for the soft-bed case with the grounding-line being 19 km farther downstream compared to its initial position (Fig. 4), resting on the last subglacial topographic high before the retrograde sloping topography would cause it to retreat to its initial position. The hysteresis

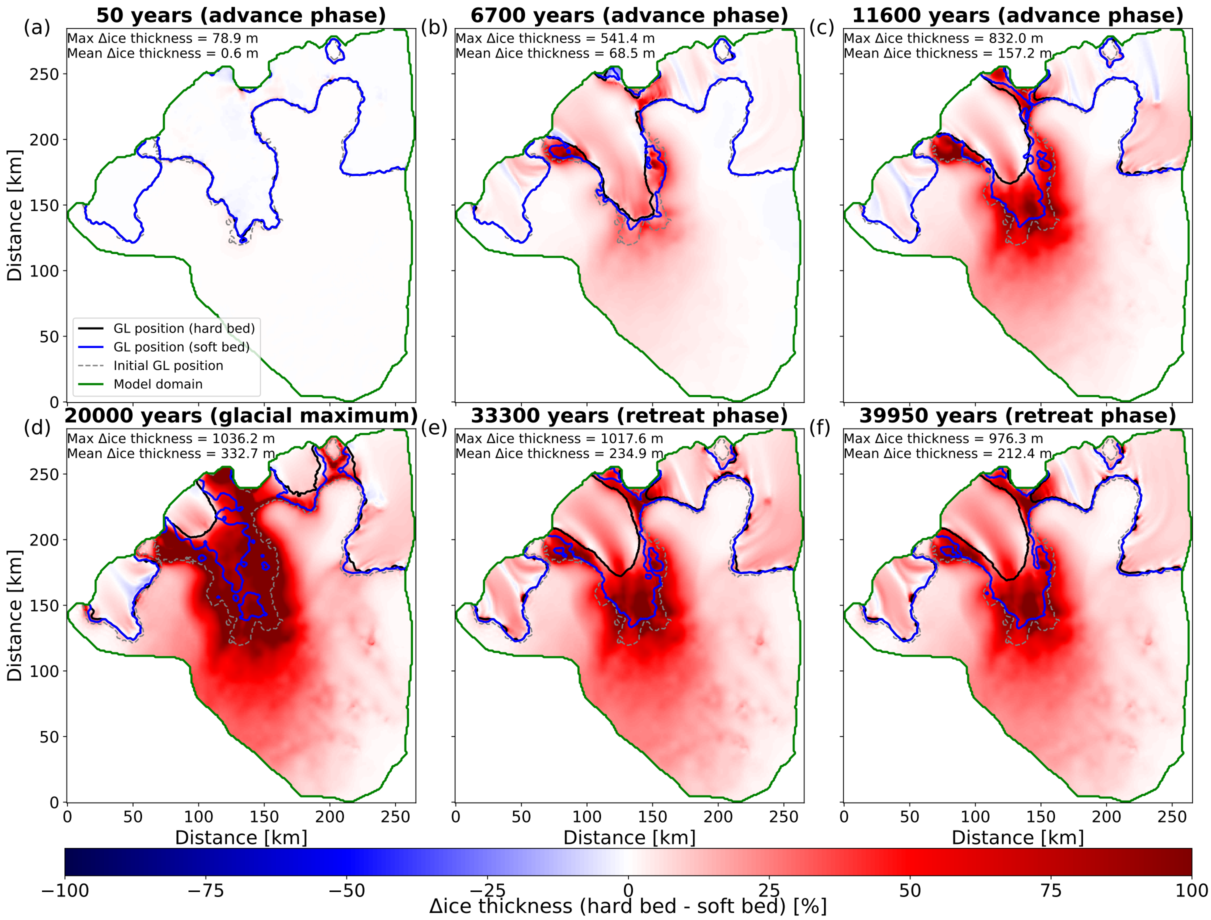

Figure 3. Differences in plan-view of ice thickness and grounding-line positions between the hard and soft-bed simulations at selected time slices. (a-d) show differences in the advance phase and (e,f) show differences in the retreat phase.

effect is much more pronounced in the hard-bed simulation in which the grounding line is 57 km downstream of its initial position (Fig. 4). This means that during the retreat phase, the grounding-line retreats only ∼39% in comparison to the simulated grounding-line advance during the retreat phase of the hard-bed simulation. Both simulations show very little retreat in the last 9,000 years of the retreat phase with grounding-line retreat magnitudes <7 km in this time span. This coincides with the period of little sea-level variations, leading us to conclude that at least for the retreat phase, sea-level forcing is the most important model forcing.

Our results underline the dependence of the final ice-sheet geometry on the model's initial state over timescales of a glacial cycle or longer. The modelled hysteresis behavior shows the non-linear response of ice-sheet evolution to very similar model forcing, a particularly challenging problem for model simulations over at least one advance and retreat cycle (Pollard & DeConto, 2009; Gasson et al., 2016). This means that the employed modelling framework will likely not result in the correct ice-sheet geometry at the LGM due to non-linear feedback mechanisms such as the marine-ice-sheet instability (Schoof, 2007; Durand et al., 2009), the height-mass balance feedback (Oerlemans, 2002), and remaining uncertainties regarding the subglacial topography.

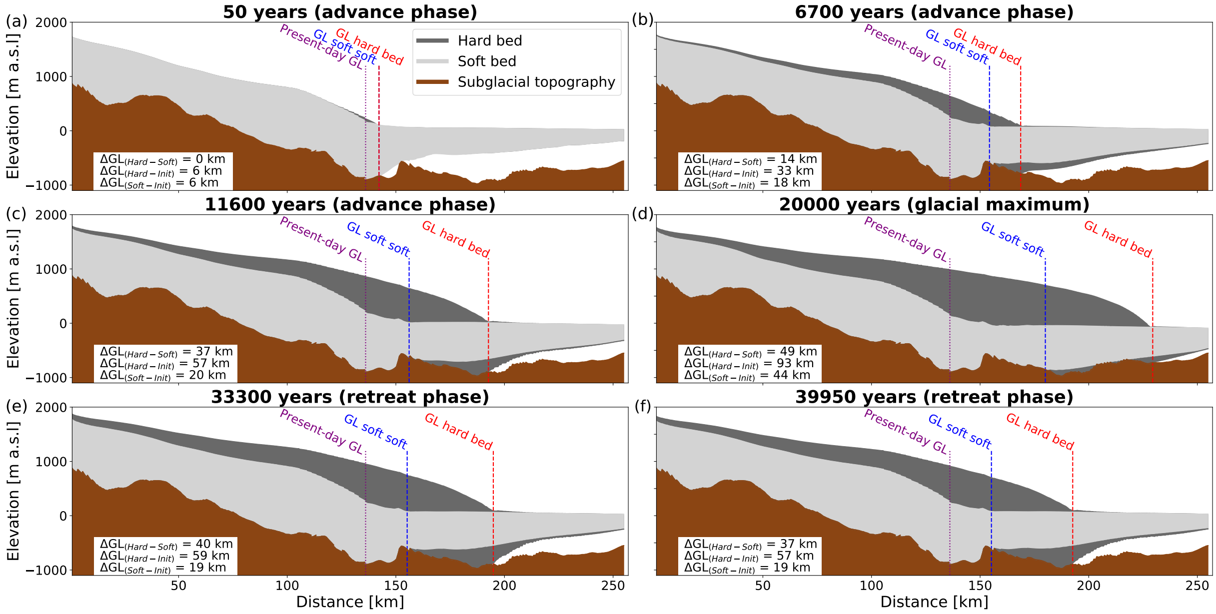

Figure 4. Difference in ice-sheet geometry and grounding-line position along a flowline (A-A' in Fig. 1) for the soft and hard-bed simulations. (a-d) show differences in the advance phase and (e,f) show differences in the retreat phase.

3.4 Model limitations

The modelling approach presented here is tailored towards capturing ice and grounding-line dynamics to high accuracy at the cost of comparatively naive parameterizations for the SMB and BMB which can be improved in the future. Also, we have not considered glacial isostatic adjustment (GIA). Until recently, GIA was considered to be only important on timescales exceeding 1,000 years. However, recent progress has revealed that due to lower than previously assumed mantle viscosities, response times of GIA to ice unloading can be as short as five years for certain sections in Antarctica (Barletta et al., 2018; Whitehouse et al., 2019). While present-day GIA rates for East Antarctica are relatively low ($\sim$1mm/yr (Martín-Español et al., 2016)) in comparison to regions of high mass loss in Antarctica, the effect over 20,000 years could amount to $\sim$20 m of elevation drop for the subglacial topography. This number is small in comparison to for example sea-level variations ($\sim$130 m), but may nevertheless result in a grounding-line position that is not as far advanced at the glacial maximum as presented in our simulations.

4 Conclusions

We investigated the effect of basal ocean bed properties on ice-sheet geometry over a full glacial cycle. We find that sediment-covered 'slippery' ocean beds result in entirely different ice-sheet geometries, ice-sheet advance and retreat patterns, and grounding-line positions in comparison to crystalline 'sticky' ocean beds. Based on our simulations in conjunction with geophysical observations (Smith et al., 2019), we think that substrate distribution (sediments vs. crystalline bedrock) on the continental shelf might be more heterogeneous than previously thought. Recent geomorphological evidence indicates that the grounding line was close to the continental shelf front at the LGM, leading us to conclude that the hard ocean bed simulation matches better with observations than the soft ocean bed simulation.

The differences between hard-bed and soft-bed simulations (>50% ice volume, >1000 m ice thickness, and >100% grounding line motion) are such that they may help to reduce the discrepancy between reconstructed sea-level drop and sea-level equivalent stored in all ice sheets at the LGM ("missing ice" problem (Clark & Tarasov, 2014)). For example, if we extrapolate our volume difference between hard and soft bed (∼50%) to the entire ice sheet at the LGM, we could reduce the discrepancy by ∼33% to ∼10 m sea-level equivalent. However, additional studies like ours are needed for other locations to establish if our results are more regionally valid, or if local conditions within each catchment lead to different results.

Owing to our new modelling setup, we reduced computation times in comparison to previous simulations by ∼80% and extended the temporal range of full-Stokes simulations by a factor of 40 compared to previous studies. Considering the uncertainties surrounding internal ice dynamics, this provides an important step forward to reduce uncertainties and brings us closer to a process-based understanding of a number of subglacial processes (e.g. glacial erosion).

Acknowledgments

Clemens Schannwell was supported by the Deutsche Forschungsgemeinschaft (DFG) grant EH329/11-1 (to TAE) in the framework of the priority programme "Antarctic Research with comparative investigations in Arctic ice areas". Reinhard Drews was funded in the same project under MA 3347/10-1. Reinhard Drews is supported by the DFG Emmy Noether grant DR 822/3-1. The authors gratefully acknowledge the Gauss Centre for Supercomputing e.V. (www.gauss-centre.eu) for providing computing time on the GCS Supercomputer SuperMUC-NG at Leibniz Supercomputing Centre (www.lrz.de). The Elmer/Ice code is publicly available through GitHub (https://github.com/ElmerCSC/elmerfem, lastaccess: 05 November 2019). All simulations were performed with version 8.3 (rev. 74a4936). Elmer/Ice scripts including all necessary input files to reproduce the simulations are available at https://doi.org/10.5281/zenodo.3564168 (Schannwell (2019), last access: 5 November 2019).

References

Albrecht, T., Winkelmann, R., & Levermann, A. (2019). Glacial cycles simulation of the Antarctic Ice Sheet with PISM - Part 2: Parameter ensemble analysis. *The Cryosphere Discuss.*, *2019*, 1–38. doi: 10.5194/tc-2019-70

Alley, R. B., Cuffey, K. M., & Zoet, L. K. (2019). Glacial erosion: status and outlook. *Annals of Glaciology*, 1–13. doi: 10.1017/aog.2019.38

Barletta, V. R., Bevis, M., Smith, B. E., Wilson, T., Brown, A., Bordoni, A., ... Wiens, D. A. (2018). Observed rapid bedrock uplift in Amundsen Sea Embayment promotes ice-sheet stability. *Science*, *360*(6395), 1335. doi: 10.1126/science.aao1447

Batchelor, C., & Dowdeswell, J. (2015). Ice-sheet grounding-zone wedges (GZWs) on high-latitude continental margins. *Marine Geology*, *363*, 65–92. doi: 10.1016/j.margeo.2015.02.001

Beckmann, A., & Goosse, H. (2003). A parameterization of ice shelf-ocean interaction for climate models. *Ocean modelling*, *5*(2), 157–170.

Bindschadler, R., Choi, H., Wichlacz, A., Bingham, R., Bohlander, J., Brunt, K., ... Young, N. (2011). Getting around Antarctica: new high-resolution mappings of the grounded and freely-floating boundaries of the Antarctic ice sheet created for the International Polar Year. *The Cryosphere*, *5*(3), 569–588. doi: 10.5194/tc-5-569-2011

Bintanja, R., van de Wal, R. S., & Oerlemans, J. (2005). Modelled atmospheric temperatures and global sea levels over the past million years. *Nature*, *437*(7055), 125–128. doi: 10.1038/nature03975

Bons, P. D., Kleiner, T., Llorens, M.-G., Prior, D. J., Sachau, T., Weikusat, I., & Jansen, D. (2018). Greenland Ice Sheet: Higher Nonlinearity of Ice Flow Significantly Reduces Estimated Basal Motion. *Geophysical Research Letters*, *45*(13), 6542–6548. doi: 10.1029/2018GL078356

Briggs, R. D., Pollard, D., & Tarasov, L. (2014). A data-constrained large ensemble analysis of Antarctic evolution since the Eemian. *Quaternary Science Reviews*, *103*, 91–115. doi: 10.1016/j.quascirev.2014.09.003

Clark, P. U., & Tarasov, L. (2014). Closing the sea level budget at the Last Glacial Maximum. *Proceedings of the National Academy of Sciences*, *111*(45), 15861. doi: 10.1073/pnas.1418970111

Comiso, J. C. (2000). Variability and Trends in Antarctic Surface Temperatures from In Situ and Satellite Infrared Measurements. *Journal of Climate*, *13*(10), 1674–1696. doi: 10.1175/1520-0442(2000)013⟨1674:VATIAS⟩2.0.CO;2

Cornford, S. L., Martin, D. F., Payne, A. J., Ng, E. G., Le Brocq, A. M., Gladstone, R. M., ... Vaughan, D. G. (2015). Century-scale simulations of the response of the West Antarctic Ice Sheet to a warming climate. *The Cryosphere*, *9*(4), 1579–1600. doi: 10.5194/tc-9-1579-2015

Drews, R., Martín, C., Steinhage, D., & Eisen, O. (2013). Characterizing the glaciological conditions at Halvfarryggen ice dome, Dronning Maud Land, Antarctica. *Journal of Glaciology*, *59*(213), 9–20. doi: 10.3189/2013JoG12J134

Durand, G., Gagliardini, O., de Fleurian, B., Zwinger, T., & Le Meur, E. (2009). Marine ice sheet dynamics: Hysteresis and neutral equilibrium. *Journal of Geophysical Research*, *114*(F3). doi: 10.1029/2008JF001170

Egholm, D. L., Knudsen, M. F., Clark, C. D., & Lesemann, J. E. (2011). Modeling the flow of glaciers in steep terrains: The integrated second-order shallow ice approximation (iSOSIA). *Journal of Geophysical Research*, *116*(F2). doi: 10.1029/2010JF001900

Favier, L., Durand, G., Cornford, S. L., Gudmundsson, G. H., Gagliardini, O., Gillet-Chaulet, F., ... Le Brocq, A. M. (2014). Retreat of Pine Island Glacier controlled by marine ice-sheet instability. *Nature Climate Change*, *4*, 117.

Fretwell, P., Pritchard, H. D., Vaughan, D. G., Bamber, J. L., Barrand, N. E., Bell, R., ... Zirizzotti, A. (2013). Bedmap2: improved ice bed, surface and thickness datasets for Antarctica. *The Cryosphere*, *7*(1), 375–393. doi: 10.5194/tc-7-375-2013

Gagliardini, O., Zwinger, T., Gillet-Chaulet, F., Durand, G., Favier, L., de Fleurian, B., ... Thies, J. (2013). Capabilities and performance of Elmer/Ice, a new-generation ice sheet model. *Geosci. Model Dev.*, *6*(4), 1299–1318. doi: 10.5194/gmd-6-1299-2013

Gasson, E., DeConto, R. M., Pollard, D., & Levy, R. H. (2016). Dynamic Antarctic ice sheet during the early to mid-Miocene. *Proceedings of the National Academy of Sciences*, *113*(13), 3459. doi: 10.1073/pnas.1516130113

Gillet-Chaulet, F., Gagliardini, O., Seddik, H., Nodet, M., Durand, G., Ritz, C., ... Vaughan, D. G. (2012). Greenland ice sheet contribution to sea-level rise from a new-generation ice-sheet model. *The Cryosphere*, *6*(6), 1561–1576. doi: 10.5194/tc-6-1561-2012

Gohl, K., Uenzelmann-Neben, G., Larter, R. D., Hillenbrand, C.-D., Hochmuth, K., Kalberg, T., ... Nitsche, F. O. (2013). Seismic stratigraphic record of the Amundsen Sea Embayment shelf from pre-glacial to recent times: Evidence for a dynamic West Antarctic ice sheet. *Marine Geology*, *344*, 115–131. doi: 10.1016/j.margeo.2013.06.011

Golledge, N. R., Fogwill, C. J., Mackintosh, A. N., & Buckley, K. M. (2012). Dynamics of the last glacial maximum Antarctic ice-sheet and its response to ocean forcing. *Proceedings of the National Academy of Sciences*, *109*(40), 16052–16056.

Graf, W., Oerter, H., Reinwarth, O., Stichler, W., Wilhelms, F., Miller, H., & Mulvaney, R. (2002). Stable-isotope records from Dronning Maud Land, Antarctica. *Annals of Glaciology*, *35*, 195–201. doi: 10.3189/172756402781816492

Herman, F., Beaud, F., Champagnac, J.-D., Lemieux, J.-M., & Sternai, P. (2011). Glacial hydrology and erosion patterns: A mechanism for carving glacial valleys. *Earth and Planetary Science Letters*, *310*(3-4), 498–508. doi: 10/fxcwgb

Herman, F., Beyssac, O., Brughelli, M., Lane, S. N., Leprince, S., Adatte, T., . . . Cox, S. C. (2015). Erosion by an Alpine glacier. *Science*, *350*(6257), 193–195.

Humphrey, N. F., & Raymond, C. F. (1994). Hydrology, erosion and sediment production in a surging glacier: Variegated Glacier, Alaska, 1982–83. *Journal of Glaciology*, *40*(136), 539–552. doi: 10.3189/S0022143000012429

Koppes, M., Hallet, B., Rignot, E., Mouginot, J., Wellner, J. S., & Boldt, K. (2015). Observed latitudinal variations in erosion as a function of glacier dynamics. *Nature*, *526*(7571), 100–103. doi: 10.1038/nature15385

Kristoffersen, Y., Hofstede, C., Diez, A., Blenkner, R., Lambrecht, A., Mayer, C., & Eisen, O. (2014). Reassembling Gondwana: A new high quality constraint from vibroseis exploration of the sub-ice shelf geology of the East Antarctic continental margin. *Journal of Geophysical Research: Solid Earth*, *119*(12), 9171–9182. doi: 10.1002/2014JB011479

Kulp, S. A., & Strauss, B. H. (2019). New elevation data triple estimates of global vulnerability to sea-level rise and coastal flooding. *Nature Communications*, *10*(1), 4844. doi: https://doi.org/10.1038/s41467-019-12808-z

Lambeck, K., Rouby, H., Purcell, A., Sun, Y., & Sambridge, M. (2014). Sea level and global ice volumes from the Last Glacial Maximum to the Holocene. *Proceedings of the National Academy of Sciences*, *111*(43), 15296–15303. doi: 10.1073/pnas.1411762111

Lenaerts, J. T., Brown, J., Van Den Broeke, M. R., Matsuoka, K., Drews, R., Callens, D., . . . Van Lipzig, N. P. (2014). High variability of climate and surface mass balance induced by Antarctic ice rises. *Journal of Glaciology*, *60*(224), 1101–1110. doi: 10.3189/2014JoG14J040

MacAyeal, D. R. (1993). A tutorial on the use of control methods in ice-sheet modeling. *Journal of Glaciology*, *39*(131), 91–98. doi: 10.3189/S0022143000015744

MacGregor, J. A., Fahnestock, M. A., Catania, G. A., Aschwanden, A., Clow, G. D., Colgan, W. T., . . . Seroussi, H. (2016). A synthesis of the basal thermal state of the Greenland Ice Sheet. *Journal of Geophysical Research: Earth Surface*, *121*(7), 1328–1350. doi: 10.1002/2015JF003803

Malinen, M., Ruokolainen, J., Råback, P., Thies, J., & Zwinger, T. (2013). Parallel Block Preconditioning by Using the Solver of Elmer. In P. Manninen & P. Öster (Eds.), *Applied Parallel and Scientific Computing* (pp. 545–547). Berlin, Heidelberg: Springer Berlin Heidelberg.

Martos, Y. M., Catalán, M., Jordan, T. A., Golynsky, A., Golynsky, D., Eagles, G., & Vaughan, D. G. (2017). Heat Flux Distribution of Antarctica Unveiled. *Geophysical Research Letters*, *44*(22), 11,417–11,426. doi: 10.1002/2017GL075609

Martín-Español, A., King, M. A., Zammit-Mangion, A., Andrews, S. B., Moore, P., & Bamber, J. L. (2016). An assessment of forward and inverse GIA solutions for Antarctica. *Journal of Geophysical Research: Solid Earth*, *121*(9), 6947–6965. doi: 10.1002/2016JB013154

Oerlemans, J. (2002). On glacial inception and orography. *Inception: Mechanisms, patterns and timing of ice sheet inception*, *95-96*, 5–10. doi: 10.1016/S1040-6182(02)00022-8

Pachauri, R. K., Allen, M. R., Barros, V. R., Broome, J., Cramer, W., Christ, R., . . . others (2014). *Climate change 2014: synthesis report. Contribution of Working Groups I, II and III to the fifth assessment report of the Intergovernmental Panel on Climate Change*. Ipcc.

Pattyn, F., & Durand, G. (2013). Why marine ice sheet model predictions may diverge in estimating future sea level rise. *Geophysical Research Letters*, *40*(16), 4316–4320. doi: 10.1002/grl.50824

Pollard, D., Chang, W., Haran, M., Applegate, P., & DeConto, R. (2016). Large ensemble modeling of the last deglacial retreat of the West Antarctic Ice Sheet: comparison of simple and advanced statistical techniques. *Geosci. Model Dev.*, *9*(5), 1697–1723. doi: 10.5194/gmd-9-1697-2016

Pollard, D., & DeConto, R. M. (2009). Modelling West Antarctic ice sheet growth and collapse through the past five million years. *Nature*, *458*(7236), 329–332. doi: 10.1038/nature07809

Rignot, E., Mouginot, J., & Scheuchl, B. (2011). Ice Flow of the Antarctic Ice Sheet. *Science*, *333*(6048), 1427–1430. doi: 10.1126/science.1208336

Ritz, C., Rommelaere, V., & Dumas, C. (2001). Modeling the evolution of Antarctic ice sheet over the last 420,000 years: Implications for altitude changes in the Vostok region. *Journal of Geophysical Research: Atmospheres*, *106*(D23), 31943–31964. doi: 10.1029/2001JD900232

Rückamp, M., Falk, U., Frieler, K., Lange, S., & Humbert, A. (2018). The effect of overshooting 1.5 °C global warming on the mass loss of the Greenland ice sheet. *Earth Syst. Dynam.*, *9*(4), 1169–1189. doi: 10.5194/esd-9-1169-2018

Schannwell, C. (2019). *Elmer/Ice simulation files for LGM simulations in "Glacial cycle ice-sheet evolution controlled by ocean bed properties".* Zenodo. Retrieved from `https://doi.org/10.5281/zenodo.3564168` doi: 10.5281/zenodo.3564168

Schannwell, C., Drews, R., Ehlers, T. A., Eisen, O., Mayer, C., & Gillet-Chaulet, F. (2019). Kinematic response of ice-rise divides to changes in ocean and atmosphere forcing. *The Cryosphere*, *13*(10), 2673–2691. doi: 10.5194/tc-13-2673-2019

Schoof, C. (2007). Ice sheet grounding line dynamics: Steady states, stability, and hysteresis. *Journal of Geophysical Research*, *112*(F3). doi: 10.1029/2006JF000664

Seddik, H., Greve, R., Zwinger, T., Gillet-Chaulet, F., & Gagliardini, O. (2012). Simulations of the Greenland ice sheet 100 years into the future with the full Stokes model Elmer/Ice. *Journal of Glaciology*, *58*(209), 427–440. doi: 10.3189/2012JoG11J177

Simms, A. R., Lisiecki, L., Gebbie, G., Whitehouse, P. L., & Clark, J. F. (2019). Balancing the last glacial maximum (LGM) sea-level budget. *Quaternary Science Reviews*, *205*, 143–153. doi: 10.1016/j.quascirev.2018.12.018

Smith, E. C., Hattermann, T., Kuhn, G., Gaedicke, C., Berger, S., Drews, R., ... Eisen, O. (2019). Detailed seismic bathymetry beneath ekstroem ice shelf, antarctica: Implications for glacial history and ice-ocean interaction. *Earth and Space Science Open Archive*. doi: 10.1002/essoar.10501125.1

Spagnolo, M., Phillips, E., Piotrowski, J. A., Rea, B. R., Clark, C. D., Stokes, C. R., ... Szuman, I. (2016). Ice stream motion facilitated by a shallow-deforming and accreting bed. *Nature Communications*, *7*(1), 10723. doi: 10.1038/ncomms10723

Tsai, V. C., Stewart, A. L., & Thompson, A. F. (2015). Marine ice-sheet profiles and stability under coulomb basal conditions. *Journal of Glaciology*, *61*(226), 205–2 15. doi: 10.3189/2015JoG14J221

Whitehouse, P. L., Bentley, M. J., & Le Brocq, A. M. (2012). A deglacial model for Antarctica: geological constraints and glaciological modelling as a basis for a new model of Antarctic glacial isostatic adjustment. *Quaternary Science Reviews*, *32*, 1–24. doi: 10.1016/j.quascirev.2011.11.016

Whitehouse, P. L., Gomez, N., King, M. A., & Wiens, D. A. (2019). Solid Earth change and the evolution of the Antarctic Ice Sheet. *Nature Communications*, *10*(1), 503. doi: 10.1038/s41467-018-08068-y

Yanites, B. J., & Ehlers, T. A. (2016). Intermittent glacial sliding velocities explain variations in long-timescale denudation. *Earth and Planetary Science Letters*, *450*, 52–61. doi: 10.1016/j.epsl.2016.06.022

Zhao, C., Gladstone, R. M., Warner, R. C., King, M. A., Zwinger, T., & Morlighem, M. (2018). Basal friction of Fleming Glacier, Antarctica – Part 1: Sensitivity of inversion to temperature and bedrock uncertainty. *The Cryosphere*, *12*(8), 2637–2652. doi: 10.5194/tc-12-2637-2018

Supporting Information for "Glacial cycle ice-sheet evolution controlled by ocean bed properties "

C. Schannwell[1], R. Drews[1], T.A. Ehlers[1], O.Eisen[2,3], C. Mayer[4], M. Malinen[5], E.C. Smith[2], and H. Eisermann[2]

[1]Department of Geosciences, University of Tübingen, Tübingen, Germany

[2]Glaciology, Alfred Wegener Institute, Helmholtz Centre for Polar and Marine Research, Bremerhaven, Germany

[3]Department of Geosciences, University of Bremen, Bremen, Germany

[4]Bavarian Academy for Sciences and Humanities, MunichCSC-IT Center for Science Ltd., Espoo, Finland, Germany

[5]CSC-IT Center for Science Ltd., Espoo, Finland

1. Stable groundging-line positions

In total there are four distinct periods in which the grounding line exhibits stability over several thousand years. Because the hard bed simulation shows larger magnitudes of grounding-line migration, we will focus on this simulation. However, while the position of the stable grounding-line differs between hard bed and soft bed simulations, the relative timing of the periods of stability are very similar, hinting that these stable configurations might be to first order controlled by a common model forcing (e.g. sea level) or boundary condition (e.g. bathymetry). Three out of modelled four stable grounding-line positions occur in the advance phase (0-20,000 years) and one occurs in the retreat phase (20,000-

40,000 years, Figure S1). However, the third stable grounding-line position is present in both periods with this particular configuration being stable for 8,000 years in the hard bed simulation (2,000 years before LGM - 6,000 years after LGM). While the specific timing of the stable grounding-line periods might not be correct due to the employed modelling approach, these modelled positions can still serve as spatial markers of areas where depositional landforms such as Grounding-Zone Wedges (GZWs) may be found.

2. Model description

2.1. Ice flow equations

Ice flow is dominated by viscous forces which permits the dropping of the inertia and acceleration terms in the linear momentum equations. The Elmer/Ice ice-sheet model (Gagliardini et al., 2013) solves the complete 3D equation for ice deformation. This results in the Stokes equations described by

$$div\boldsymbol{\sigma} = -\rho_i \boldsymbol{g}. \tag{1}$$

Here, $\boldsymbol{\sigma} = \boldsymbol{\tau} - p\boldsymbol{I}$ is the Cauchy stress tensor, $\boldsymbol{\tau}$ is the deviatoric stress tensor, $p = -tr(\boldsymbol{\sigma})/3$ is the isotropic pressure, $\boldsymbol{I}$ the identity tensor, ρ_i the ice density, and $\boldsymbol{g}$ is the gravitational vector. Ice flow is assumed to be incompressible which simplifies mass conservation to

$$div\boldsymbol{u} = 0, \tag{2}$$

with $\boldsymbol{u}$ being the ice velocity vector. Here we model ice as an isotropic material. Its rheology is given by Glens flow law which relates the deviatoric stress $\boldsymbol{\tau}$ with the strain rate $\dot{\boldsymbol{\epsilon}}$:

$$\boldsymbol{\tau} = 2\eta\dot{\boldsymbol{\epsilon}}, \tag{3}$$

where the effective viscosity η can be expressed as

$$\eta = \frac{1}{2} E B \dot{\boldsymbol{\epsilon}}_{\boldsymbol{e}}^{\frac{(1-n)}{n}}. \quad (4)$$

In this equation E is the enhancement factor, B is a viscosity parameter that depends on ice temperature relative to the pressure melting point computed through an Arrhenius law, n is Glens flow law parameter (n=3), and the effective strain rate is defined as $\dot{\epsilon_e}^2 = tr(\dot{\boldsymbol{\epsilon}}^{\boldsymbol{2}})/2$. In all our simulations E is set to 1 which means that ice is modelled as an isotropic material.

2.2. Ice temperature

The ice temperature is determined through the heat transfer equation (e.g. Gagliardini et al., 2013) which reads

$$\rho c_v \left(\frac{\partial T}{\partial t} + \boldsymbol{u} \cdot T \right) = div(\kappa gradT) + \boldsymbol{D} : \boldsymbol{\sigma}, \quad (5)$$

where c_v and κ are the specific heat of ice and the heat conductivity, respectively. The $:$ operator represents the colon product between two tensors. This last term of the equation represents strain heating.

2.3. Boundary conditions

2.3.1. Ice temperature

Our parameterisation of surface temperature changes follows Ritz et al. (2001). We parameterise relative surface temperature changes to present-day as a function of relative surface elevation change with respect to present-day elevations and a spatially uniform surface temperature variation that is derived from the nearby EDML ice core. The surface temperature is then given by (Ritz et al. (2001), eq. 11):

$$T_a = T_{a0} - 0.00914(z_{s0} - z_s) + \Delta T_{clim}. \tag{6}$$

Here T_a and T_{a0} are the surface temperatures at the current timestep and present-day (from Comiso (2000)), z_s and z_{s0} are the surface elevations at the current timestep and present-day, and ΔT_{clim} is the climatic forcing derived from the EDML ice core. As in Ritz et al. (2001), we apply a spatially constant lapse rate of 0.00914°C/m (Table S1).
At the grounded underside of the ice sheet, where the ice in contact with the subglacial topography, we prescribe the geothermal heat flux (Martos et al., 2017). This heat flux is time invariant. Ice temperature is set to the local pressure melting point for the boundary condition underneath the floating ice shelves.

2.3.2. Surface mass balance (SMB) and basal mass balance (BMB)

A kinematic boundary condition determines the evolution of upper and lower surfaces z_j:

$$\frac{\partial z_j}{\partial t} + u_x \frac{\partial z_j}{\partial x} + u_y \frac{\partial z_j}{\partial y} = u_z + \dot{a}_j, \tag{7}$$

where $\dot{a}_j$ is the accumulation/ablation term and $j = (b, s)$, with s being the upper surface and b being the lower surface (base) of the ice sheet.
For the surface mass balance (SMB) parameterisation, we closely follow Ritz et al. (2001) again. However, we assume that no melt occurs in all our simulations. As for the surface temperature, our SMB parameterisation uses a present-day distribution of the SMB (Lenaerts et al., 2014) as input. Variations of the SMB over time are then proportional to the exponential of the surface temperature variation (Ritz et al. (2001), eq. 12):

$$\dot{a}_s(T_a) = \dot{a}_{s0}(T_{a0}) exp(\Delta a \cdot (T_a - T_{a0})), \tag{8}$$

where a_{s0} is the present-day SMB, a_s is the SMB at the current timestep, and the parameter $\Delta a = 0.07°\mathrm{C}^{-1}$. This means that for a surface temperature drop of 10°C, the SMB is reduced by 50% (Ritz et al., 2001).

Sub-shelf melting underneath the floating ice shelves is based on the difference between the local freezing point of water under the ice shelves and the ocean temperature near the continental shelf break (Beckmann & Goosse, 2003). The freezing temperature (T_f) is calculated through:

$$T_f = 0.0939 - 0.057 S_o + 7.64 \times 10^{-4} z_b, \tag{9}$$

where S_o is the ocean salinity (Table S1). The basal melt rates ($\dot{a}_b$) are then computed by

$$\dot{a}_b = \frac{\rho_w c_{p_o} \gamma_T F_{melt} (T_O - T_f)^2}{L \rho_i}. \tag{10}$$

In this equation, ρ_w is the density of water, c_{p_o} is the specific capacity of the ocean mixed layer, γ_T is the thermal exchange velocity, L is the latent heat capacity of ice, F_{melt} is a tuning parameter to match present day melt rates, and T_O is the ocean temperature (Table S1). The ocean temperature is initially set to -0.52°C (Beckmann & Goosse, 2003). Applied variations of the ocean temperature are a damped (∼40%) and delayed (∼3,000 years) version of the climatic forcing for surface temperature ΔT_{clim} (Bintanja et al., 2005).

2.3.3. Basal sliding and sea-level

Where the ice is in contact with the subglacial topography a linear Weertman-type sliding law of the form

$$\boldsymbol{\tau_b} = C |\boldsymbol{u_b}|^{m-1} \boldsymbol{u_b}, \tag{11}$$

is employed. Here $\boldsymbol{\tau_b}$ is the basal traction, m is the basal friction exponent which is set to 1 in all simulations, and C is the basal friction coefficient. For the present-day grounded ice sheet, C is inferred by solving an inverse problem (see section 2.4), and for the present-day ocean beds a uniform basal friction coefficient of 10^{-1} MPa m^{-1} yr and 10^{-5} MPa m^{-1} yr is prescribed for the soft (sediment-based) bed and hard (crystalline rock-based) bed simulations. Underneath the floating part of the domain basal traction is zero ($\boldsymbol{\tau_b} = 0$), but hydrostatic sea pressure is prescribed.

We initialise the present-day sea-level to zero and apply sea-level variations according to Lambeck et al. (2014).

2.4. Model initialisation

The model is initialised to the present-day geometry using the commonly applied snapshot initialisation in which the basal traction coefficient C is inferred by matching observed ice velocities with modelled ice velocities. The same optimisation parameters as in Schannwell et al. (2019) are used. Similar to Zhao et al. (2018), we employ a two-step initialisation scheme. In the first iteration, the optimisation problem is solved with an isothermal ice sheet with ice temperature set to -10°C. The resulting velocity field is then used to solve the steady-state temperature equation before the optimisation problem is solved again with the new temperature field. This type of temperature initialisation approach should provide similar results to a computationally expensive temperature spin-up over several glacial cycles (Rückamp et al., 2018), as long as the system is close to steady state. There is growing evidence that this is the case for the Ekström Ice Shelf catchment (e.g. Drews et al., 2013; Schannwell et al., 2019).

2.5. Mesh generation and refinement

We initially create a 2D isotropic mesh with a nominal mesh resolution of ∼6 km everywhere in the domain. To ensure that we simulate grounding-line dynamics at the required detail, we use the meshing software MMG (http://www.mmgtools.org/, last access: 2 October 2019) to locally refine the mesh down to ∼1 km in the region of present-day Ekstöm Ice Shelf (Figure S2) with areas away from the region of interest remaining at ∼6 km resolution. The mesh is then vertically extruded, consisting of 10 layers and held fixed in time.

2.6. ParStokes

Because of the non-Newtonian rheology of ice and the dependence of viscosity on ice velocity, the resulting Stokes equations are non-linear and have to be solved iteratively. In three dimensions the arising systems of linear equations become large (10^6-10^7 degrees of freedom) very quickly. Standard iterative methods (Krylov supspace methods) in conjunction with algebraic preconditioners (e.g. Incomplete LU (ILU) decomposition) do not converge for most real-word geometries in glaciology. High aspect ratios of the finite elements and spatial viscosity variations of several orders of magnitudes, strongly affect accuracy and stability of the numerical solution (Malinen et al., 2013). This means that most glaciology application with Elmer/Ice revert to using a direct method for solving the Stokes equations. While robust, direct solvers do not take advantage of the sparse structure of the matrix and require large amounts of memory. In three dimensions their memory requirements increase with the square of the number of unknowns. Therefore, we use a stable parallel iterative solver (ParStokes) in our simulations that is implemented in Elmer/Ice, but has so far been rarely used. ParStokes is based on the idea of block preconditioning (Malinen et al., 2013) that improves the solvability of the underlying saddle-point problem (via clustering of eigenvalues) such that Krylov subspace methods now converge. This results in a much better scaling of the required computation time with increasing numbers of Computer Processing Units (CPUs, Figure S3). For our simulations, the ParStokes solver is about 71-84% faster than the "classic" Elmer/Ice setup that uses a direct solver (Figure S4). As our problem size with ∼570,000 degrees of freedom is of medium size, there might be even more speed-up potential for larger problems by using more CPUs.

3. Reduction of computation time with the ParStokes solver

Full-Stokes simulations in 3D have thus far been restricted to timescales that are shorter than 1,000 years due to their high computational demands (Seddik et al., 2012; Favier et al., 2014; Schannwell et al., 2019). Simpler model variants omit one or several stress gradients in the underlying ice-flow equations, with partially unknown consequences for, for example, grounding-line migration behavior. It is therefore required to extent the simulation times of full-Stokes models. The vast majority of the computation time is spent on solving the non-linear equations for ice velocity. Here, we compare simulations of Elmer/Ice using the classic velocity solver setup employing a parallelized direct solver to a so far unused stable parallel iterative solver setup. The total compute time for the iterative solver is 80% faster. In our case this means that the 40,000-year simulation now takes 23 days instead of 141 days for the hard-bed case, and 27 days instead of 94 days for the soft-bed case (Figure S4). The time differences between both scenarios are due to the differing grounding-line migration pattern, which require additional computation time for the hard-bed case. This significant speed-up unlocks a new time dimension for the applicability of 3D full-Stokes ice-sheet models on the regional scale while keeping a high mesh resolution. Our modelling approach using the complete mechanical model for ice flow together with a freely evolving grounding line without parameterisations can now be combined with simplified ice-sheet models using ensemble simulations (Briggs et al., 2014; Pollard et al., 2016). This provides an important step in reducing uncertainties regarding internal ice dynamics, a key process to a better understanding of grounding-line dynamics and processes occurring at the underside of the ice sheet.

4. Comparison between direct Stokes solver (MUMPS) and ParStokes

To ensure that the "classic" solver setup using the direct Solver MUMPS and the new iterative solver ParStokes provide the similar results, we compare grounding-line positions over time for the hard bed and soft bed simulations in this section. We note however that we do not expect a perfect match between the two solver setups due to small differences in the finite element formulation (e.g. stabilization method).

For both simulations, there is very good agreement in terms of grounding-line position over time, with differences never exceeding 5% (Figure S5). Because the soft bed simulation exhibits smaller magnitude grounding-line motion over the simulation, agreement between the two solver setups is better, with differences well below 1% for almost the entire simulation length. In the hard bed simulation, where larger magnitudes of grounding-line motion are modelled, the ParStokes solver's grounding-line is not as far advanced as the MUMPS solver grounding-line (Figure S6). Moreover, at times of rapid grounding-line motion, the response of the grounding-line in the ParStokes solver is delayed. This leads to certain differences in transient grounding-line positions (<5%). However, the situation improves for steady state grounding-line positions (<1.5% difference).

The larger variations in grounding-line position coupled with the more extreme geometrical changes in the case of different grounding-line positions in the hard bed simulation also result in larger differences in ice thickness. Locally these differences can be as large as ∼460 m (<25% of the ice thickness). These differences are pronounced in the periods of delayed grounding-line response, but reduce once a stable grounding-line position has been reached (Figure S6, S7).

5. Grounding-line flux calculation

To compute present-day ice flux across the grounding line, we extract ice thickness from Bedmap2 (Fretwell et al., 2013) and ice velocities from the MEaSURES product (Rignot et al., 2011) along the present-day grounding line (Bindschadler et al., 2011). We then define the threshold for slower moving catchments as ≤300m/yr and compute the ice flux (velocity · ice thickness) and the percentage area that belongs to the category of slower moving catchments. This shows that 90% of the present-day Antarctic grounding-line is occupied by slower moving catchments and they account for ∼30% of the total ice flux across the grounding line.

6. Effect of ocean bed properties on estimated erosion rate

Due to our modelling approach, we have reduced uncertainties regarding the magnitude of basal sliding. However, significant uncertainties remain for basal processes such as erosion which we demonstrate in this section.

Erosion rates are commonly linked to the magnitude of basal sliding to some power (e.g. Herman et al., 2015; Koppes et al., 2015). This means that differences in basal properties (e.g. basal friction) of ocean beds affect computed erosion rates. Differences in basin-averaged erosion rates using two recently proposed erosion laws (Herman et al., 2015; Koppes et al., 2015) alone can be significant (up to 0.021 mm/yr). However, while the uncertainties surrounding the selected erosion law are already large, the effect of differing ocean bed properties is even larger (Figure S8). Even though absolute differences appear small when averaged over the basin ($\leq$0.022 mm/yr), when these mean erosion rates (10^{-7}-10^{-5} mm/yr for hard bed and $4{\cdot}10^{-5}$-$8{\cdot}10^{-4}$ mm/yr for soft bed) are used to estimate erosion volumes over a glacial cycle the variations are significant. This is a consequence of each time step contributing to the increasing difference, so that the cumulative effect becomes even larger (two orders of magnitude for the two different ocean bed simulations, Figure S8c). Erosion volumes are between $9.65{\cdot}10^3$-$5.46{\cdot}10^5$ m^3 for the hard bed and $1.28{\cdot}10^6$-$2.11{\cdot}10^7$ m^3 for the soft bed over the full glacial cycle.

This simple calculation assumes that all sediment is instantly eroded and no sediment transport takes place. Absolute numbers might be different, but the magnitude of the effect of different ocean bed properties on basal sliding velocities and erosion volumes will not change. This underlines the importance of an improved understanding of how much of ice flow is caused by internal deformation or basal sliding.

References

Beckmann, A., & Goosse, H. (2003). A parameterization of ice shelf-ocean interaction for climate models. *Ocean modelling*, *5*(2), 157–170.

Bindschadler, R., Choi, H., Wichlacz, A., Bingham, R., Bohlander, J., Brunt, K., ... Young, N. (2011). Getting around Antarctica: new high-resolution mappings of the grounded and freely-floating boundaries of the Antarctic ice sheet created for the International Polar Year. *The Cryosphere*, *5*(3), 569–588. doi: 10.5194/tc-5-569-2011

Bintanja, R., van de Wal, R. S., & Oerlemans, J. (2005). Modelled atmospheric temperatures and global sea levels over the past million years. *Nature*, *437*(7055), 125–128. doi: 10.1038/nature03975

Briggs, R. D., Pollard, D., & Tarasov, L. (2014). A data-constrained large ensemble analysis of Antarctic evolution since the Eemian. *Quaternary Science Reviews*, *103*, 91–115. doi: 10.1016/j.quascirev.2014.09.003

Comiso, J. C. (2000). Variability and Trends in Antarctic Surface Temperatures from In Situ and Satellite Infrared Measurements. *Journal of Climate*, *13*(10), 1674–1696. doi: 10.1175/1520-0442(2000)013⟨1674:VATIAS⟩2.0.CO;2

Drews, R., Martín, C., Steinhage, D., & Eisen, O. (2013). Characterizing the glaciological conditions at Halvfarryggen ice dome, Dronning Maud Land, Antarctica. *Journal of Glaciology*, *59*(213), 9–20. doi: 10.3189/2013JoG12J134

Favier, L., Durand, G., Cornford, S. L., Gudmundsson, G. H., Gagliardini, O., Gillet-Chaulet, F., ... Le Brocq, A. M. (2014). Retreat of Pine Island Glacier controlled by marine ice-sheet instability. *Nature Climate Change*, *4*, 117.

Fretwell, P., Pritchard, H. D., Vaughan, D. G., Bamber, J. L., Barrand, N. E., Bell, R., ... Zirizzotti, A. (2013). Bedmap2: improved ice bed, surface and thickness datasets for Antarctica. *The Cryosphere*, *7*(1), 375–393. doi: 10.5194/tc-7-375-2013

Gagliardini, O., Zwinger, T., Gillet-Chaulet, F., Durand, G., Favier, L., de Fleurian, B., … Thies, J. (2013). Capabilities and performance of Elmer/Ice, a new-generation ice sheet model. *Geosci. Model Dev.*, *6*(4), 1299–1318. doi: 10.5194/gmd-6-1299-2013

Herman, F., Beyssac, O., Brughelli, M., Lane, S. N., Leprince, S., Adatte, T., … Cox, S. C. (2015). Erosion by an Alpine glacier. *Science*, *350*(6257), 193–195.

Koppes, M., Hallet, B., Rignot, E., Mouginot, J., Wellner, J. S., & Boldt, K. (2015). Observed latitudinal variations in erosion as a function of glacier dynamics. *Nature*, *526*(7571), 100–103. doi: 10.1038/nature15385

Lambeck, K., Rouby, H., Purcell, A., Sun, Y., & Sambridge, M. (2014). Sea level and global ice volumes from the Last Glacial Maximum to the Holocene. *Proceedings of the National Academy of Sciences*, *111*(43), 15296–15303. doi: 10.1073/pnas.1411762111

Lenaerts, J. T., Brown, J., Van Den Broeke, M. R., Matsuoka, K., Drews, R., Callens, D., … Van Lipzig, N. P. (2014). High variability of climate and surface mass balance induced by Antarctic ice rises. *Journal of Glaciology*, *60*(224), 1101–1110. doi: 10.3189/2014JoG14J040

Malinen, M., Ruokolainen, J., Råback, P., Thies, J., & Zwinger, T. (2013). Parallel Block Preconditioning by Using the Solver of Elmer. In P. Manninen & P. ster (Eds.), *Applied Parallel and Scientific Computing* (pp. 545–547). Berlin, Heidelberg: Springer Berlin Heidelberg.

Martos, Y. M., Cataln, M., Jordan, T. A., Golynsky, A., Golynsky, D., Eagles, G., & Vaughan, D. G. (2017). Heat Flux Distribution of Antarctica Unveiled. *Geophysical Research Letters*, *44*(22), 11,417–11,426. doi: 10.1002/2017GL075609

Pollard, D., Chang, W., Haran, M., Applegate, P., & DeConto, R. (2016). Large ensemble modeling of the last deglacial retreat of the West Antarctic Ice Sheet: comparison of simple and advanced statistical techniques. *Geosci. Model Dev.*, *9*(5), 1697–1723. doi: 10.5194/gmd-9-1697-2016

Rignot, E., Mouginot, J., & Scheuchl, B. (2011). Ice Flow of the Antarctic Ice Sheet. *Science*, *333*(6048), 1427–1430. doi: 10.1126/science.1208336

Ritz, C., Rommelaere, V., & Dumas, C. (2001). Modeling the evolution of Antarctic ice sheet over the last 420,000 years: Implications for altitude changes in the Vostok region. *Journal of Geophysical Research: Atmospheres*, *106*(D23), 31943–31964. doi: 10.1029/2001JD900232

Rückamp, M., Falk, U., Frieler, K., Lange, S., & Humbert, A. (2018). The effect of overshooting 1.5 °C global warming on the mass loss of the Greenland ice sheet. *Earth Syst. Dynam.*, *9*(4), 1169–1189. doi: 10.5194/esd-9-1169-2018

Schannwell, C., Drews, R., Ehlers, T. A., Eisen, O., Mayer, C., & Gillet-Chaulet, F. (2019). Kinematic response of ice-rise divides to changes in ocean and atmosphere forcing. *The Cryosphere*, *13*(10), 2673–2691. doi: 10.5194/tc-13-2673-2019

Seddik, H., Greve, R., Zwinger, T., Gillet-Chaulet, F., & Gagliardini, O. (2012). Simulations of the Greenland ice sheet 100 years into the future with the full Stokes model Elmer/Ice. *Journal of Glaciology*, *58*(209), 427–440. doi: 10.3189/2012JoG11J177

Zhao, C., Gladstone, R. M., Warner, R. C., King, M. A., Zwinger, T., & Morlighem, M. (2018). Basal friction of Fleming Glacier, Antarctica Part 1: Sensitivity of inversion to temperature and bedrock uncertainty. *The Cryosphere*, *12*(8), 2637–2652. doi:

10.5194/tc-12-2637-2018

Table S1. Numerical values of the parameters adopted for the simulations

Parameter	Symbol	Value	Unit
ice density	ρ_i	917	kg m^{-3}
ocean density	ρ_w	1028	kg m^{-3}
Glen's exponent	n	3	
Gravity	g	9.81	m s^{-2}
Enhancement factor	E	1	
Tuning parameter SMB	Δacc	0.07	C^{-1}
Ocean salinity	S_0	35.0	PSU
Heat capacity	c_{p_o}	3974	J kg^{-1} C^{-1}
Latent heat of fusion	L	3.35×10^{-4}	J kg^{-1}
Tuning parameter BMB	F_{melt}	0.383×10^{-4}	
Thermal exchange velocity	γ_T	1×10^{-5}	m s^{-1}

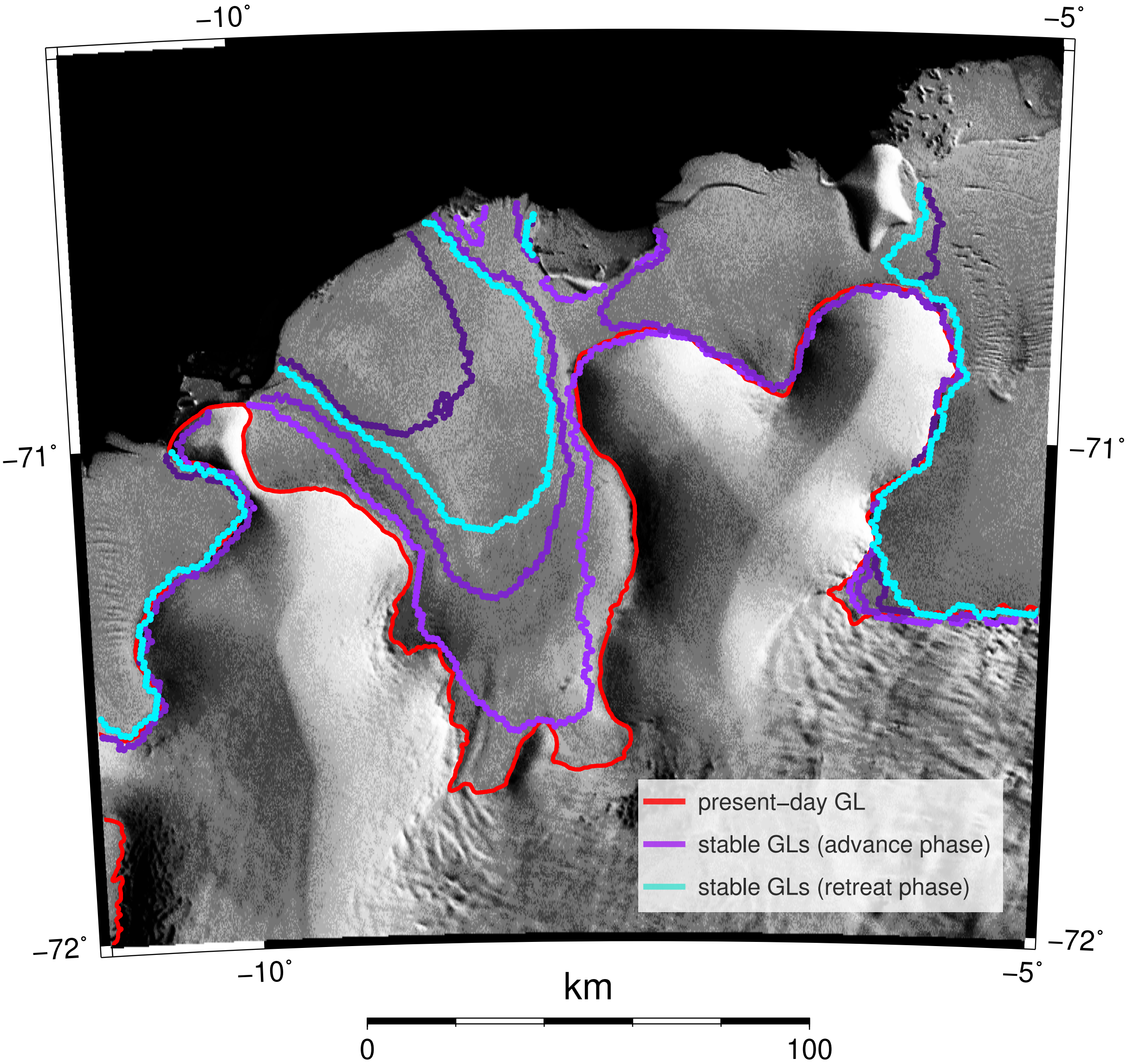

Figure S1. Modelled stable grounding-line positions from present-day back to the LGM (purple lines, advance phase) and from the LGM back to present day (cyan line, retreat phase).

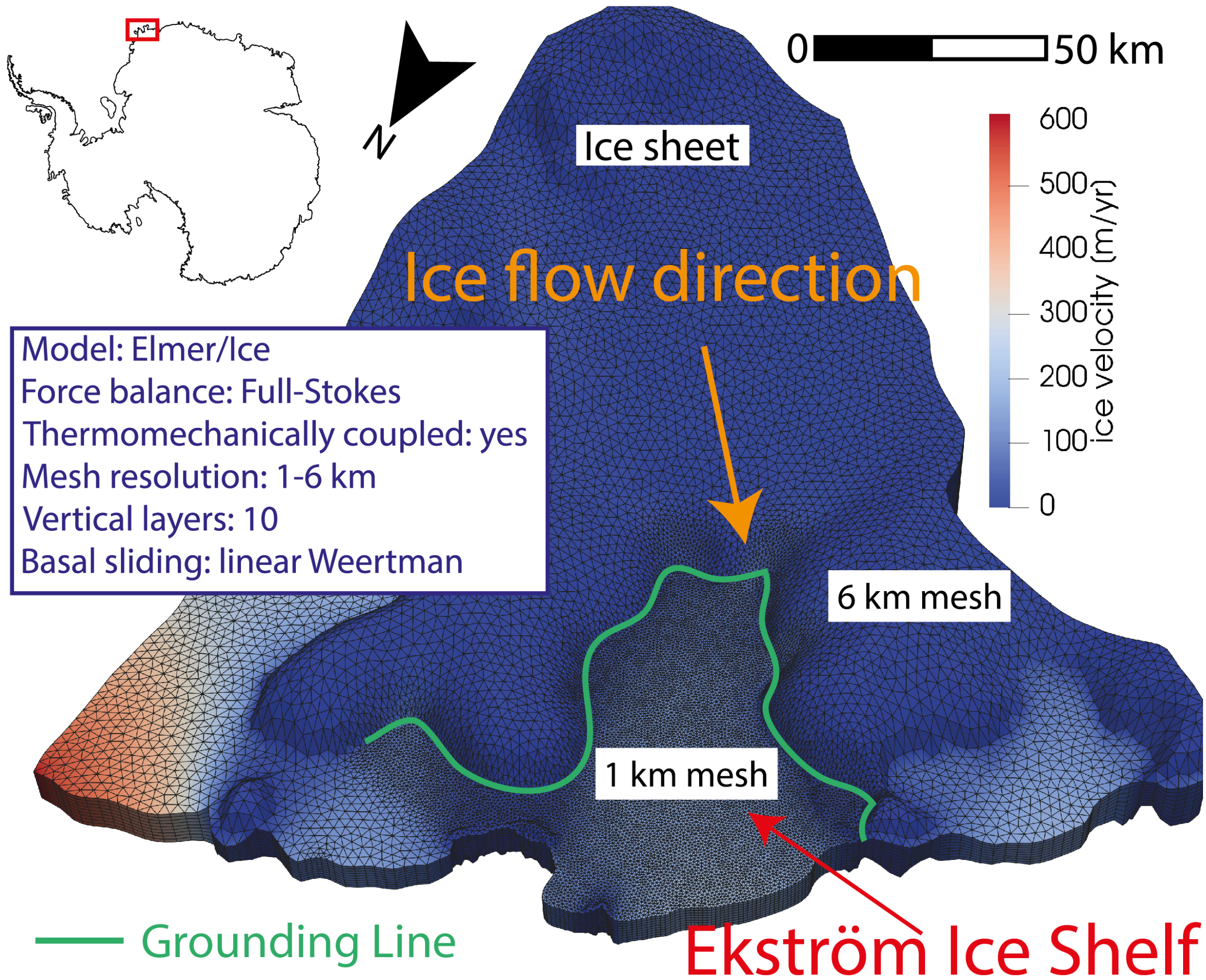

Figure S2. Model domain in 3D including numerical mesh of Ekström Ice Shelf catchment, East Antarctica

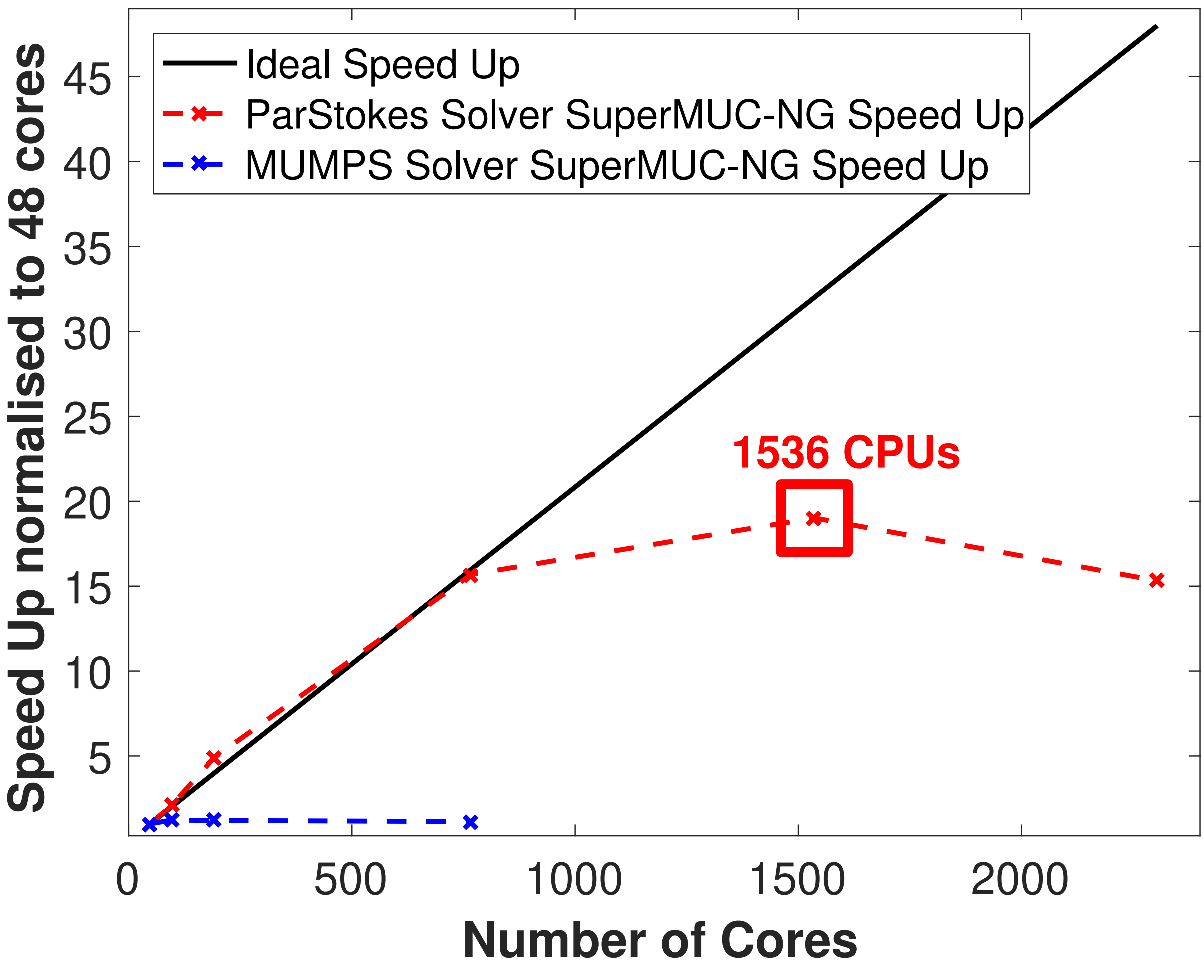

Figure S3. Scaling behaviour of iterative solver (ParStokes) and direct Solver (MUMPS) for Elmer/Ice on the SuperMUC-NG supercomputer in Munich.

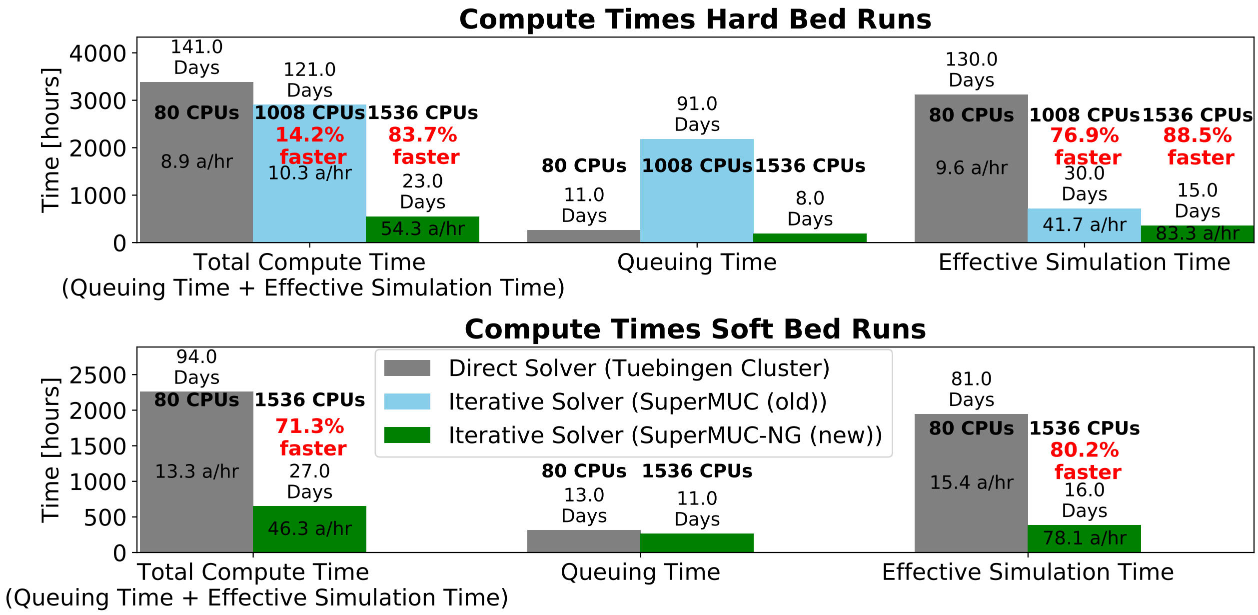

Figure S4. Speed-up of iterative Solver (ParStokes, green bars) in comparison to direct solver (MUMPS, gray bars) for the hard bed cavity (upper panel) and soft bed cavity (lower panel) simulations.

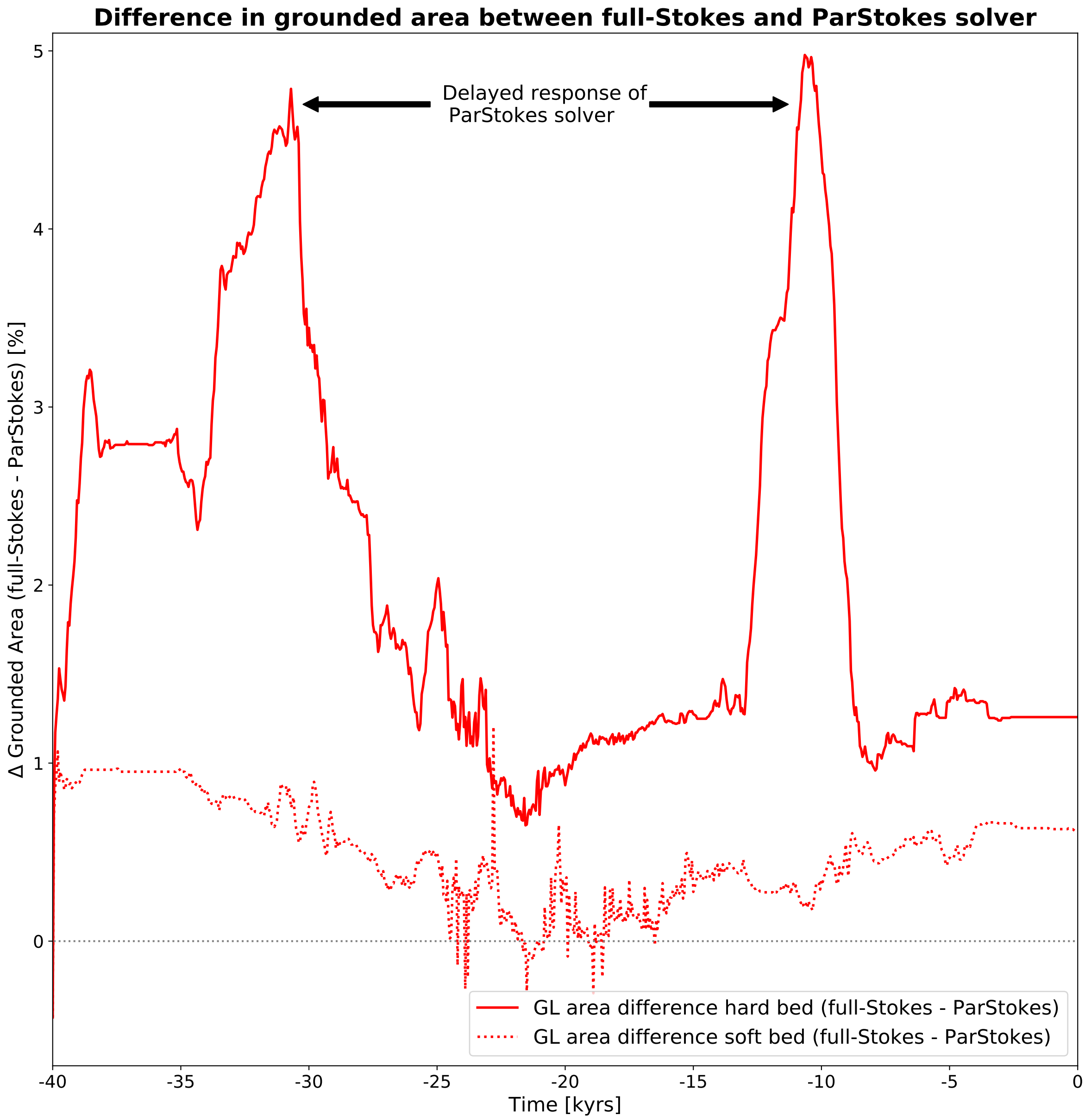

Figure S5. Differences in grounding-line (GL) area between the classic MUMPS and ParStokes solver setup for the soft bed and hard bed simulations.

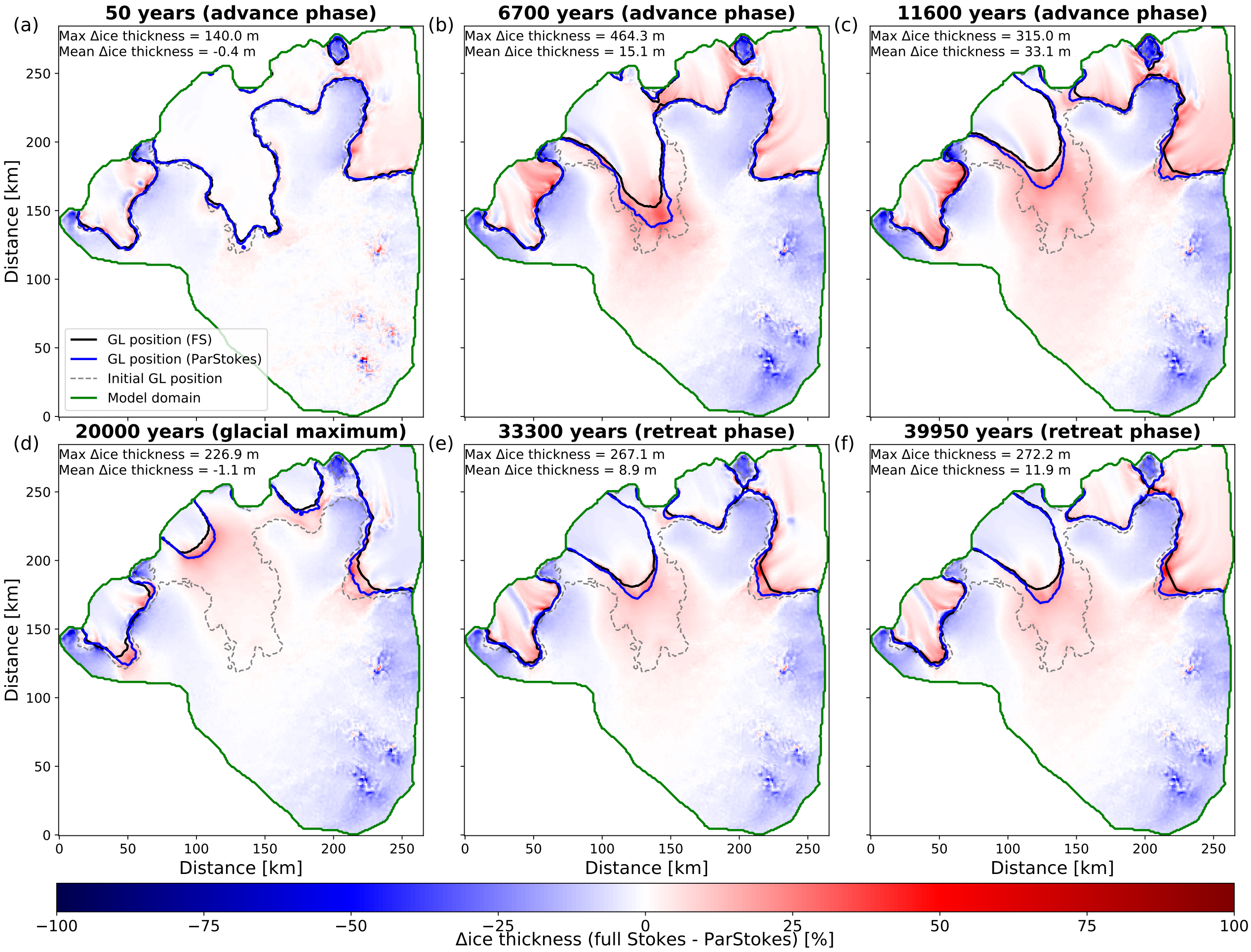

Figure S6. Differences in grounding-line position and ice thickness between the classic MUMPS and ParStokes solver setup for the hard bed simulation at specific time slices.

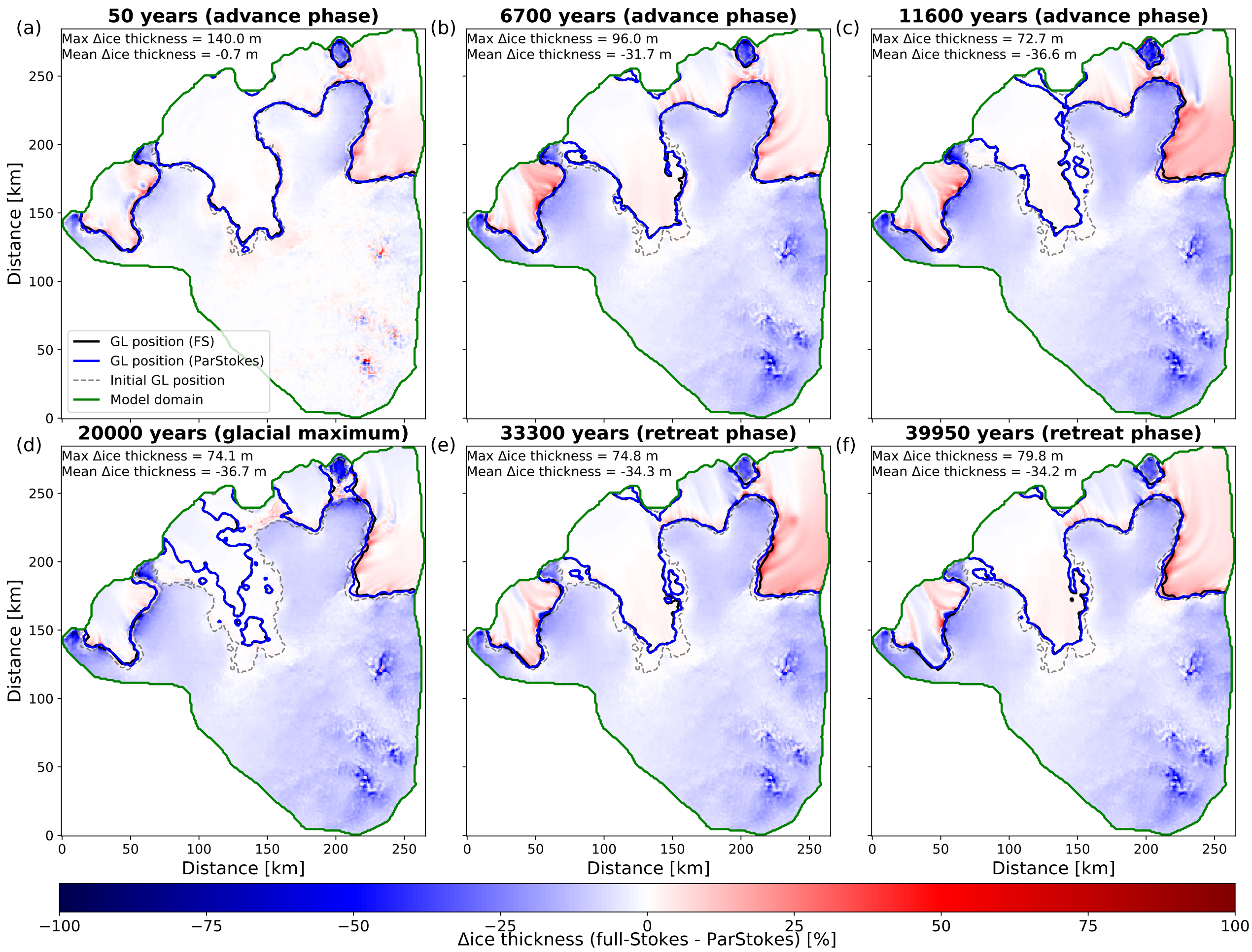

Figure S7. Differences in grounding-line position and ice thickness between the classic MUMPS and ParStokes solver setup for the soft bed simulation at specific time slices.

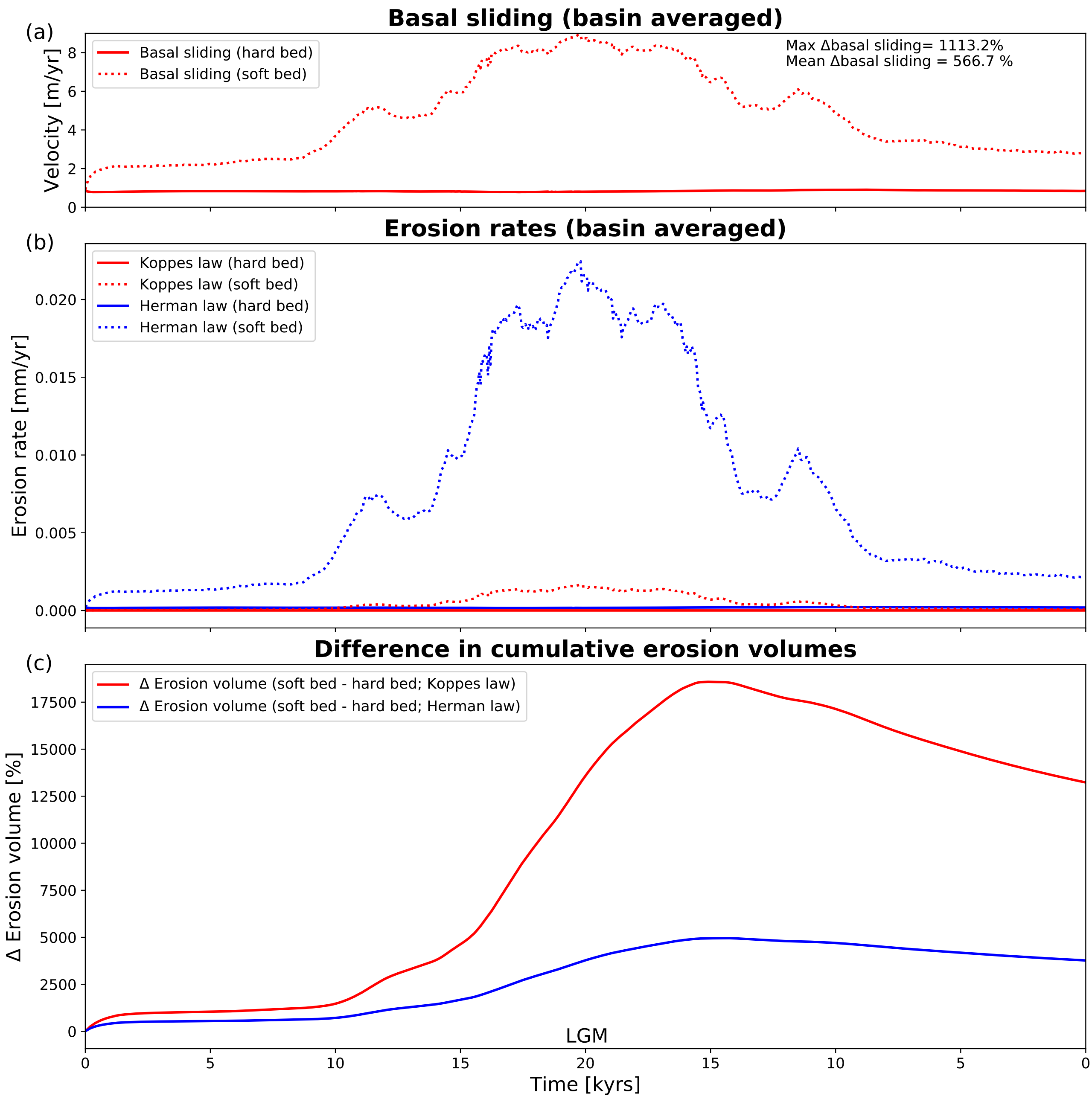

Figure S8. (a) basal sliding, (b) erosion rates, and (c) differences in cumulative erosion volumes for the hard bed and soft bed simulations using two different erosion laws.